Chair of Mechanics

Master's Thesis

Implementation of the Heterosegmental PC-SAFT Approach

Clara Gessl, BA BSc

May 2023

MONTANUNIVERSITÄT LEOBEN
www.unileoben.ac.at

EIDESSTATTLICHE ERKLÄRUNG

Ich erkläre an Eides statt, dass ich diese Arbeit selbständig verfasst, andere als die angegebenen Quellen und Hilfsmittel nicht benutzt, und mich auch sonst keiner unerlaubten Hilfsmittel bedient habe.

Ich erkläre, dass ich die Richtlinien des Senats der Montanuniversität Leoben zu "Gute wissenschaftliche Praxis" gelesen, verstanden und befolgt habe.

Weiters erkläre ich, dass die elektronische und gedruckte Version der eingereichten wissenschaftlichen Abschlussarbeit formal und inhaltlich identisch sind.

Datum 30.05.2023

Unterschrift Verfasser/in
Clara Gessl

Abstract

The accurate prediction of thermodynamic properties of systems in thermodynamic equilibrium is crucial for the design of efficient processes in the chemical industry. The model employed in this thesis is the heterosegmental Perturbed Chain Statistical Associating Fluid Theory equation of state (PC-SAFT). PC-SAFT is a widely used thermodynamic model, which is especially suited to describe the behavior of complex fluids and associating substances. The heterosegmental approach of PC-SAFT allows for separation of molecules into various segments which are each characterized by a set of model parameters.

The model was utilized to predict the behavior of butane - alcohol systems, revealing that the two-phase region widens with an increasing number of C-atoms on the alcohol and narrows with higher temperatures. Furthermore, the mixture approaches the behavior of an ideal solution as the number of carbon atoms increases. When modeling butanol - alkane systems, it was observed that the two-phase region narrows with increasing temperature, but no widening trend was observed with an increase in the number of carbon atoms in the alkane.

The application of the model to predict the behavior of binary n-alcohol - carbon dioxide (CO_2) systems revealed limited accuracy in modeling the complete miscibility gap. Although the results show no significant improvement over the results obtained with the homosegmental approach, the heterosegmental approach offers the advantage of a single temperature-dependent binary parameter for all CO_2 - alcohol systems, whereas the homosegmental approach requires fitting multiple parameters for each unique system. While neither approach precisely predicts the vapor-liquid equilibria across the entire temperature and pressure range, the heterosegmental approach yields comparable or superior outcomes with the convenience of fitting a single binary parameter.

Additionally, it was demonstrated that the modeling results for ethane - butanol and propane - butanol systems also exhibit deviations near the critical region, akin to those observed in CO_2 - alcohol systems.

Kurzfassung

Die Vorhersage und Modellierung thermodynamischer Eigenschaften von Systemen im Gleichgewicht ist von großer Bedeutung für die Auslegung und Gestaltung effizienter Prozesse in der chemischen Industrie. Das in dieser Arbeit verwendete Modell ist die heterosegmentelle Perturbed Chain Statistical Associating Fluid Theory (PC-SAFT). PC-SAFT ist ein weit verbreitetes Modell für Zustandsgleichungen, das besonders gut geeignet ist, das Verhalten komplexer Fluide und assoziierender Substanzen zu beschreiben. Der heterosegmentelle PC-SAFT Ansatz differenziert Moleküle in verschiedene Segmente, die jeweils durch einen Satz von Parametern charakterisiert sind.
In der vorliegenden Arbeit wurde das Modell verwendet, um das Verhalten von Butan-Alkohol-Systemen vorherzusagen, wobei gezeigt werden konnte, dass das Zweiphasengebiet mit zunehmender Anzahl von C-Atomen im Alkohol größer wird und sich mit höheren Temperaturen verengt. Darüber hinaus nähert sich die Mischung mit zunehmender Anzahl von C-Atomen dem Verhalten einer idealen Lösung an. Für Butanol-Alkan-Systeme konnte gezeigt werde, dass das Zweiphasengebiet ebenfalls mit steigender Temperatur schrumpft.
Die Anwendung des Modells zur Vorhersage des Verhaltens von binären Alkohol - Kohlendioxid (CO_2)-Systemen zeigt, dass die Modellierung nicht im gesamten Druckbereich gut mit den experimentellen Daten übereinstimmt. Obwohl die Ergebnisse keine signifikante Verbesserung gegenüber den mit dem homosegmentellen Ansatz erzielten Ergebnissen zeigen, bietet der heterosegmentelle Ansatz den Vorteil eines einzigen temperaturabhängigen binären Parameters für alle CO_2-Alkohol-Systeme, während der homosegmentelle Ansatz eine Anpassung des Parameters für jedes einzelne System erfordert. Obwohl keiner der Ansätze in der Lage ist, die Phasengleichgewichte über den gesamten Temperatur- und Druckbereich genau vorherzusagen, liefert der heterosegmentelle Ansatz vergleichbare oder sogar bessere Ergebnisse mit dem Vorteil, dass nur ein einziger binärer Parameter angepasst werden muss.
Zusätzlich wurde gezeigt, dass die Modellierungsergebnisse für Ethanol-Butanol- und Propan-Butanol-Systeme ebenfalls Abweichungen in der Nähe der kritischen Region aufweisen, ähnlich wie bei CO_2-Alkohol-Systemen beobachtet.

Acknowledgements

At this point, I would like to express my gratitude to Dr.techn. Nagl, for his guidance, support and unwavering patience throughout the entire process of conducting this thesis. I would also like to extend my thanks to Univ.-Prof. Zeiner for his valuable insights and feedback which greatly contributed to the final shape of this thesis. Furthermore, I would like to thank Assoz. Prof. Gamsjäger for his scientific advice, as well as his inspiring curiosity and flexibility.
Lastly, I want to thank my family and friends for their support, understanding, and encouragement throughout this thesis and for lending me chargers wherever I need them.

Contents

1. Introduction

Accurate prediction of thermodynamic properties can aid in the selection of appropriate equipment, optimization of operating conditions, and design of new materials. However, there is no universally valid model that can provide precise results for the phase equilibria of all substances under all conditions, and the choice of the applied prediction method depends on the considered substances, the area of application and the desired qualities, like the required accuracy, predictive ability, or the computational speed. Over time, a wide range of models have been developed that can be broadly classified into two categories: Activity coefficient models and equations of state. Activity coefficient models describe the non-ideal behavior of mixtures by introducing the concept of activity coefficients, equations of state are mathematical models that describe the thermodynamic behavior of pure substances and mixtures in terms of their pressure, volume, and temperature. They are based on the fundamental principles of thermodynamics and statistical mechanics.

The model employed in this thesis is the Perturbed Chain Statistical Associating Fluid Theory, short PC-SAFT [1]. PC-SAFT is a widely used equation of state model in chemical engineering and thermodynamics. It was developed in the early 2000s as an improvement over the earlier SAFT equation of state (Statistical Associating Fluid Theory [2]). The model is based on statistical mechanics and uses a perturbation theory approach to capture the intermolecular interactions between molecules in the fluid. It is especially suited to predict the thermodynamic properties of complex fluids and associating substances which exhibit significant deviations from ideal behavior. In PC-SAFT, molecules are modeled as chains of spherical segments which are characterized by a set of parameters. For mixtures an additional binary interaction parameter is introduced, which characterizes the deviation of the mixture's dispersion energy from the geometric mean of the pure substances' dispersion energy.
The task of this thesis was the implementation of the heterosegmental PC-SAFT approach [3]. In comparison to the homosegmental approach, which assumes the molecules consist of identical spheres of equal size, the heterosegmental approach allows for the differentiation of molecules into various segments. This division reflects the composition of molecules like n-alcohols, which consist of an alkyl-residue and the hydroxyl group. In the heterosegmental approach, the binary interaction parameter can be defined between each part of the molecules present in a mixture.

In the chemical industry, alcohol - CO_2 systems are used in various applications, such as extraction, purification, and separation processes. Accurately predicting the thermody-

namic properties of these systems is particularly challenging due to the associating nature of alcohols and the presence of polar moments in CO_2 molecules. Ramirez et al. [4] demonstrated that the homosegmental PC-SAFT approach is not capable of predicting the vapor- liquid equilibria of these systems adequately over the entire pressure and composition range and raised the question, whether an improvement of the predictive ability of the model can be obtained by introducing a second binary interaction parameter. The heterosegmental approach provides the framework for two binary parameters used to correct the dispersion energy of the alcohol - CO_2 mixture, one between the alkyl residue and CO_2 and the other between the head segment ($-CH_2OH$) and CO_2. In order to evaluate the performance of the heterosegmental approach for predicting the behavior of alcohol - CO_2 systems, in the context of this thesis a comprehensive comparison is conducted between the results obtained with this approach and experimental data available in the literature, as well as with results obtained with the homosegmental approach.

2. State of the Art

The following chapter provides a theoretical framework for the PC-SAFT model and the calculation of phase equilibria and thermodynamic properties, introducing the basic concepts and mathematical methods which are necessary to understand the model and its application.

2.1. Thermodynamic equilibrium

The discipline of thermodynamics deals with energy, heat and a system's ability to do work [5]. In classical thermodynamics, systems are described in terms of measurable physical quantities, like temperature, pressure and volume. The principles of classical thermodynamics are based on a set of laws, such as the first and second law of thermodynamics, which describe the conservation of energy, the transfer of heat, and the direction of thermodynamic processes.
Equilibrium thermodynamics describe the state of a system in thermodynamic equilibrium. When a system is in a state of thermodynamic equilibrium no macroscopic flows of matter or energy occur within the system or from one system to another and the state variables are constant [6]. Thermodynamic equilibrium is therefore characterized as thermal, mechanical and chemical equilibrium in a system.

- **Thermal equilibrium** describes the state of a system in which the temperature is homogenous and where there are no macroscopic heat flows. As shown in equation 2.1, the temperature T must be the same for all phases (α, β,...,θ) in the considered system.

$$T^{\alpha} = T^{\beta} = ... = T^{\theta} \tag{2.1}$$

- **Mechanical equilibrium** is a state where the sum of all forces acting on a system is zero. It is characterized by the equality of pressure p in all phases.

$$p^{\alpha} = p^{\beta} = ... = p^{\theta} \tag{2.2}$$

- A system reaches a state of **chemical equilibrium** if the chemical potentials μ for each component i in all ocurring phases of the system are equal:

$$\mu_i^{\alpha} = \mu_i^{\beta} = ... = \mu^{\theta} \tag{2.3}$$

  The chemical potential is a measure of the stability of substances or their tendency

to change [7]. In an incompressible multicomponent system, the chemical potential corresponds to the partial derivative of the Gibbs energy G with respect to the amount of substance n_i when pressure and temperature are held constant, and thus describes the change in Gibbs energy per mole or per particle. In a single-component system, the chemical potential of the substance is identical to the molar Gibbs energy of the system.

$$\mu_i = \left(\frac{\partial G}{\partial n_i}\right)_{p,T,n_{j\neq i}} \tag{2.4}$$

Similarly, the chemical potential in a multicomponent system can be defined for the Helmholtz energy A. The chemical potential μ_i of component i can be expressed as the partial derivative of the Helmholtz energy A with respect to the amount of substance n_i, when temperature and volume are held constant:

$$\mu_i = \left(\frac{\partial A}{\partial n_i}\right)_{T,V,nj\neq i} \tag{2.5}$$

While thermodynamic equilibrium can occur in a single phase or multiple phases of a system, the term **phase equilibrium**, on the other hand, specifically refers to the condition where two or more phases of a substance coexist in thermodynamic equilibrium.

2.2. State variables

State variables are physical variables that describe the current macroscopic state of a system, regardless of how this state came about [6]. A system is a limited area in space to which the investigation is intended to relate. The boundaries of the system are not defined by physical conditions but are chosen according to the requirements of the calculation. Three forms of systems can be distinguished depending on the system's interaction with its environment:

- In **isolated systems** there is no flow of matter and energy over the boundary of the system.
- In **closed systems** there is no flow of matter over the boundary of the system, but there is a flow of energy.
- In **open systems** there is a flow of matter and energy over the boundary of the system.

Examples for state variables are volume, pressure and temperature, as well as internal energy, enthalpy, Helmholtz free energy, Gibbs free energy, entropy and isobaric and

isochoric heat capacities. State variables are distinguished according to their dependence on the size of the system:

- **Extensive state variables** depend on the size of the system and are proportional to the considered amount of matter in this system. (e.g. mass, volume, enthalpy...)
- **Intensive state variables** are independent from the size of the system. (e.g. pressure, temperature, density...)

Extensive state variables can be transformed into intensive variables by dividing the extensive variable through the mass or the amount of the substance.
The number of intensive state variables that can be arbitrarily changed simultaneously without destroying the equilibrium between the phases and without changing the number of phases of the system corresponds to the degrees of freedom given by the Gibbs phase rule:

$$\text{degrees of freedom} = \text{number of components} - \text{number of phases} + 2 \tag{2.6}$$

2.3. Phase diagrams

A phase diagram is a graphical representation of the equilibrium phases of a substance or mixture as a function of temperature, pressure, and composition [6]. It shows the regions of stability for each phase (solid, liquid, gas) and the conditions (pressure, temperature, and composition) at which phase transitions occur between them. The phase diagram shows the relationship between these variables and provides a useful tool for understanding and predicting the behavior of a substance under different conditions. Examples of phase diagrams are $p-T$ diagrams, where the pressure of the system is plotted as a function of the temperature at constant volume, $p-V$ diagrams, where the pressure is plotted as a function of the volume at constant temperature, or $p-x$ and $T-x$ diagrams, where respectively the pressure or temperature is plotted as a function of composition. In general, the composition is indicated for the more volatile component and is typically given on a scale from zero to one.

Figure 2.1a shows a temperature-composition phase diagram for a binary mixture. Above the dew curve, the system exists as a homogeneous gas phase, below the bubble point curve as a homogeneous liquid phase. An example of a pressure-composition phase diagram is illustrated in figure 2.1b. Here, the system is a homogeneous liquid phase at high pressures, above the bubble point curve, and a homogeneous vapor phase below the dew curve. In binary phase diagrams, the two-phase region refers to a specific region where two distinct phases coexist in equilibrium. In the given example, the dew curve and the bubble point curve meet at the boiling point of pure component 1 and the boiling

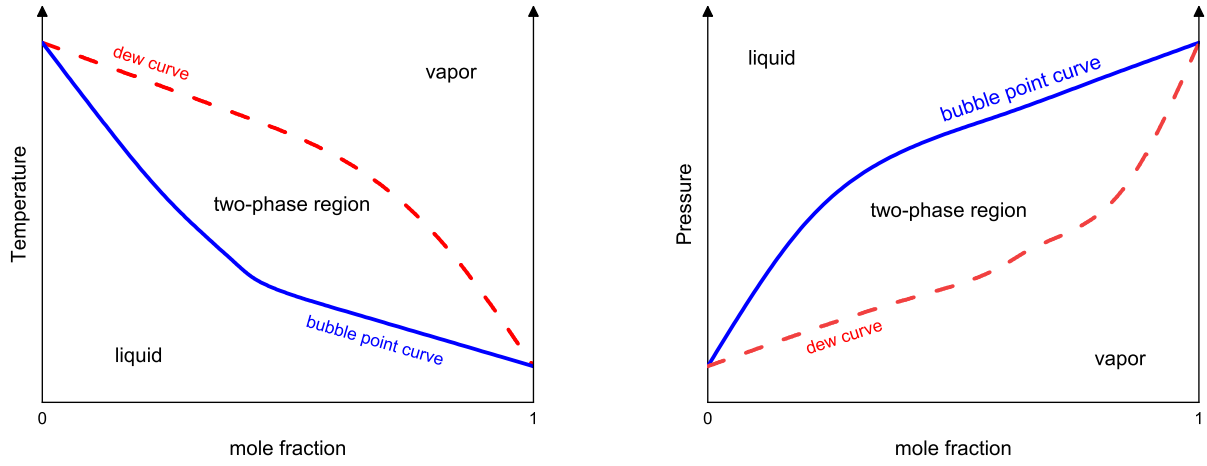

(a) $T - x$ phase diagram

(b) $p - x$ phase diagram

Figure 2.1.: Schematic illustration of an arbitrary (a) temperature-composition phase diagram and an arbitrary (b) pressure-composition phase diagram for binary systems.

point of pure component 2.

In ideal solutions, where intermolecular forces are absent, the vapor pressure follows Raoult's law, resulting in a straight line connecting the vapor pressures of pure component 1 and pure component 2. The absence of intermolecular forces allows for ideal mixing behavior, where the vapor pressure of each component is directly proportional to its mole fraction in the liquid phase. Therefore, the shape of the line reflects deviations from ideal behavior.

Another important concept is the **critical point**. In the case of pure substances, it corresponds to the temperature and pressure at which the liquid and gaseous phases combine to form a single phase, a so-called **supercritical fluid**. The **critical temperature** and **critical pressure** are the specific conditions at which this phase transition occurs. In pressure-temperature diagrams, the critical point is represented as the termination point of a phase equilibrium curve. In a pressure-volume diagram, a critical point is located on an isotherm that exhibits an inflection point with a horizontal tangent.

2.4. Statistical Thermodynamics

Statistical thermodynamics, closely related to statistical mechanics, is a branch of thermodynamics that uses the laws of statistics to explain the behavior of thermodynamic systems on a microscopic level [6]. It provides a framework for understanding the thermodynamic properties of systems in terms of the behavior of their individual particles,

such as atoms and molecules. The macroscopic quantities of compounds are derived by considering translation, rotation and oscillation of individual particles. The set of physical properties of all particles is called the microstate of the system. For systems which consist of a large number of particles, the properties of the particles can be determined with statistical methods and distributions of position and momenta. The microstate of the system changes constantly due to the motion of the particles, however, if the mean values remain the same, the observable macroscopic state of the system (pressure, temperature, volume) is constant. Each macrostate is realizable by a certain number of microstates. This number defines the thermodynamic probability of the macrostate. In thermodynamics it is assumed that all microstates with the same total energy hold the same probability.
Statistical thermodynamics makes use of the concept of the partition function, which provides a way to calculate the probability of the system being in a particular macrostate [8]. The partition function, denoted by the symbol Q, is defined as the sum or integral of the Boltzmann factor over all possible energy microstates of the system.

$$Q = \sum_i e^{\left(-\frac{E_i}{k_B T}\right)} \tag{2.7}$$

Here, E_i is the total energy of the system in the microstate i, k_B is Boltzmann's constant, and T is the temperature of the system. The partition function can be used to calculate various thermodynamic properties, such as the entropy, internal energy, and free energy of a system. For example, the internal energy U can be calculated as the sum of the energy of each state multiplied by its probability:

$$U = \frac{1}{Q} \sum_i (E_i e^{\left(-\frac{E_i}{k_B T}\right)}) \tag{2.8}$$

Similarly, the entropy S can be calculated as:

$$S = k_B \ln(Q) \tag{2.9}$$

If the partition function of a fluid is known, it is possible to calculate its thermodynamic properties exactly. However, the definition of the partition function requires knowledge of the intermolecular interactions between all the molecules in the system (see chapter 2.5.2), which can be extremely complex and difficult to model, especially for highly non-ideal fluids.

2.5. Molecular Interactions

As atoms and molecules consist of charged particles, electromagnetic forces account for attraction and repulsion between them [8]. At short distances, repulsive forces prevail. At long distances, attractive forces take over, decreasing as the distance between the molecules increases. Intermolecular forces determine the physical properties of molecules, like their melting and boiling point, their density dependent on the temperature, the respective enthalpies of fusion and vaporizationas well as their ability to form mixtures with other substances. They are also responsible for effects such as surface tension, capillarity, and adhesion and cohesion forces.

2.5.1. Types of intermolecular forces

Dependent on the composition of the considered molecule, the intermolecular forces are usually categorized as follows [8]:

- **Repulsive interactions** occur when the valence orbitals of two molecules overlap. This phenomenon is described by the Pauli exclusion principle, which states that an orbital cannot be occupied by more than two electrons. If an orbital is occupied by two electrons, their spin must be oppositional [9].

- **Electrostatic interactions** occur between the partially positively charged part and the partially negatively charged part of molecules. This applies to molecules that hold for example a permanent dipole (e.g. ketones) or quadrupole (e.g. CO_2), as they consist of covalently bonded atoms with large differences in electronegativity. **Hydrogen bonding** is a special form of dipole-dipole interaction and occurs between a covalently bonded hydrogen atom and an atom with bigger electronegativity, especially oxygen, nitrogen, or fluorine. Hydrogen bonding is the strongest form of intermolecular interaction and leads to an increased melting and boiling point, relative to the molar mass, of substances able to form hydrogen bonds, such as water, alcohols, or acids.

- **London dispersion forces** are weak forces of attraction that arise from spontaneous fluctuations in electron density. This creates an electric dipole moment in one molecule, which induces another dipole moment in a neighboring molecule. The magnitude of attraction increases with the number of involved electrons. London forces exist between all types of molecules and thus the existence of liquid and solid state for non-polar substances can be explained.

- **Induction** or **polarization** is a hybrid form and describes the interaction between a molecule with a permanent multipole and a molecule in which a spontaneous

polarization is induced.

Figure 2.2 shows a qualitative comparison of the intermolecular interaction strength or bond energy for different categories of interactions. In **simple fluids**, dispersion forces

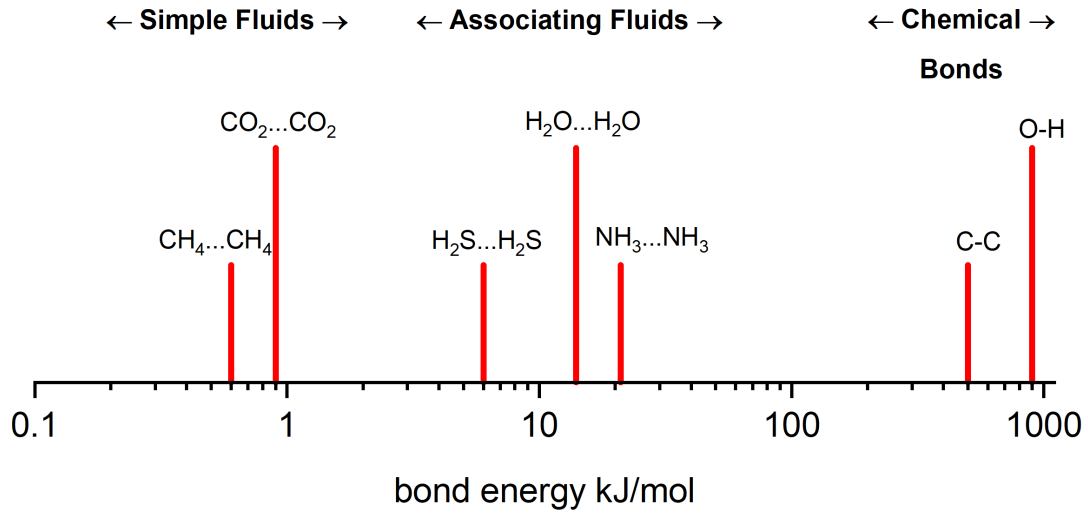

Figure 2.2.: Qualitative comparison of intermolecular interaction strength, according to [10]

prevail, which are comparatively weak. **Associative interaction** between molecules is an interaction which is highly directional and short ranged [11]. The term is used to describe electrostatic interactions in substances with polar components or components with the ability to form hydrogen bonds. The formation of hydrogen bonds between molecules of the same kind is described as self-association, while cross-association refers to the formation of hydrogen-bonds between unlike molecules. The strong intramolecular interactions between atoms within a molecule are so-called **chemical bonds**.

2.5.2. Intermolecular potentials

Molecular interactions can be described mathematically in the form of intermolecular potentials. Intermolecular potentials describe the potential energy between two or more interacting atoms or molecules as a function of the distance between the particles. Positive values of the potential correspond to a repulsive interaction, negative values to attraction.

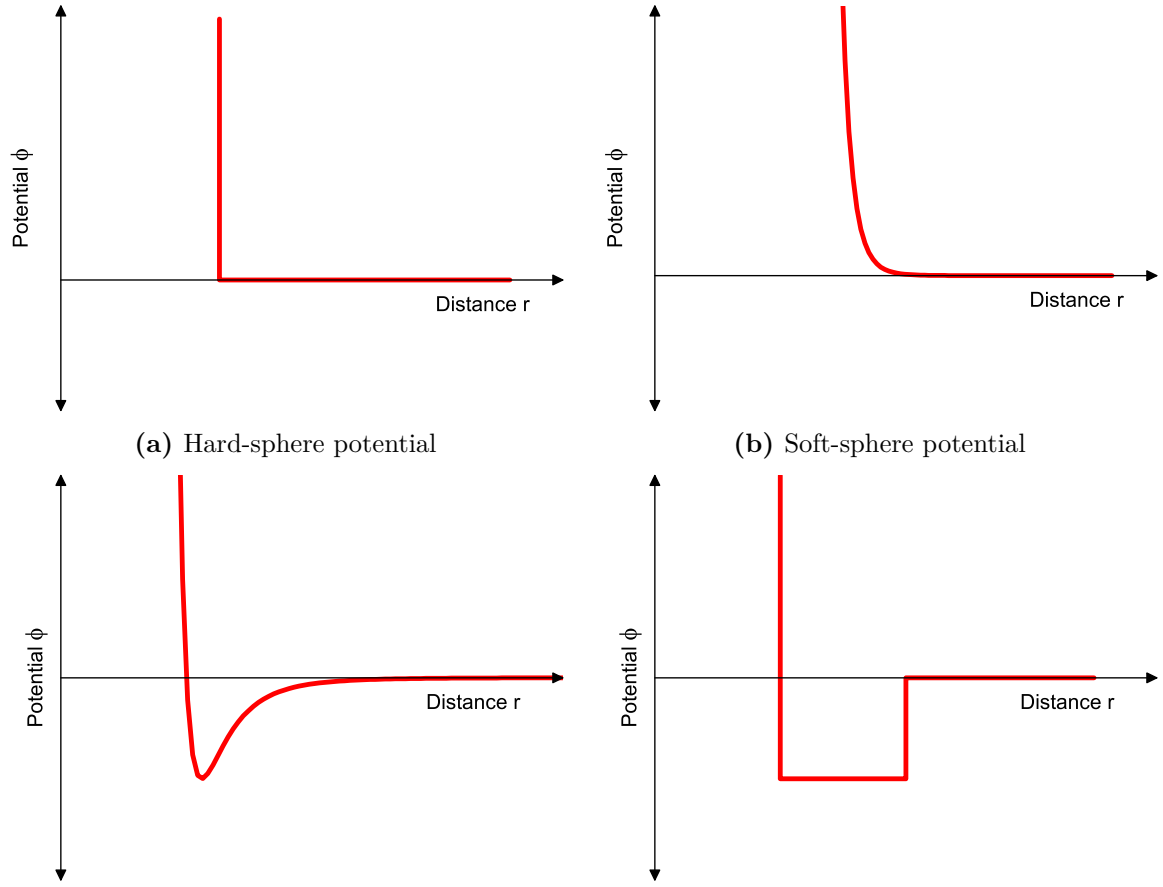

(a) Hard-sphere potential

(b) Soft-sphere potential

(c) Lennard-Jones potential

(d) Square-well potential

Figure 2.3.: Schematic graphs illustrating four types of intermolecular potentials as a function of the radial distance.

The simplest model of intermolecular potential is the **hard-sphere** or **hard-core model** [12]. It accounts for the repulsive forces between molecules by modeling them as incompressible hard-core spheres that cannot overlap in space. Attractive forces are not considered. The hard-sphere pair potential Φ_{ij} between two molecules or atoms i and j is given in equation 2.10:

$$\Phi_{ij}(r) = \begin{cases} 0 & \text{if} \quad r \geq \sigma \\ \infty & \text{if} \quad r < \sigma \end{cases} \tag{2.10}$$

Where r indicates the distance between the cores of two molecules or atoms i and j, $|\mathbf{r}_i - \mathbf{r}_j|$, σ the hard-core diameter. Figure 2.3a shows the hard-sphere potential as a function of the distance.

The hard-sphere repulsion is only physically correct when particles collide at infinitely slow speed. To model elastic diameters which become smaller during collision the **soft-sphere**

potential was introduced [13]:

$$\Phi_{ij}(r) = \begin{cases} 0 & \text{if} \quad r \geq \sigma \\ \epsilon \left(\frac{\sigma}{r}\right)^n & \text{if} \quad r < \sigma \end{cases} \tag{2.11}$$

ϵ is the interaction energy. The case of $n \to \infty$ corresponds to the hard-sphere potential. Figure 2.3b illustrates the soft-sphere potential as a function of the distance r between the cores of the considered particles.
The total intermolecular pair potential is calculated as the sum of the intermolecular potential due to repulsive forces and the potential due to attractive forces. The **Lennard-Jones potential** considers repulsive as well as attractive forces and is widely used because of its simplicity [14]. The pair potential is expressed as follows:

$$\Phi_{ij}(r) = 4\epsilon \left[\left(\frac{\sigma}{r}\right)^{12} - \left(\frac{\sigma}{r}\right)^{6} \right] \tag{2.12}$$

In this case, σ is not the molecular diameter, but the distance between the cores of two particles at which the intermolecular potential Φ_{ij} becomes zero. The maximum energy of attraction ϵ occurs at $r = 2^{\frac{1}{6}}\sigma$. At this distance, the particles experience the strongest attraction. The Lennard-Jones potential as a function of r is illustrated in figure 2.3c.
Another model which incorporates repulsive and attractive molecular interactions is the **square-well potential** [15]. In the square-well potential, the initial hard-sphere repulsion is followed by an attractive potential well. Attraction between two molecules occurs, if their relative distance is between σ, the particle diameter, and $\lambda\sigma$ (cf. figure 2.3d). λ factors the width of the attractive well.
Square-well potentials are applied to model short-range interactions between molecules, like hydrogen bonds. Their potential is given by:

$$\Phi_{ij}(r) = \begin{cases} 0 & \text{if} \quad r \geq \lambda\sigma \\ \epsilon & \text{if} \quad \sigma \leq r < \lambda\sigma \\ \infty & \text{if} \quad r < \sigma \end{cases} \tag{2.13}$$

2.6. Modeling of thermodynamic properties

There are two main types of thermodynamic models or approaches available to predict the thermodynamic properties of a substance or mixture in phase equilibrium, **activity**

coefficient models and **equations of state**.

2.6.1. Activity coefficient models

Activity coefficient models are methods to predict the activity coefficient, which accounts for the non-ideal behavior of mixtures. These models typically involve empirical correlations or theoretical models that describe the deviations from ideality, and are often based on thermodynamic concepts such as excess Gibbs energy or excess enthalpy. Some examples of activity coefficient models include Wilson, NRTL, UNIQUAC, and UNIFAC [16].
The activity coefficient γ is a dimensionless quantity that describes the deviation of a solution from ideality. It is a measure of the non-ideal behavior of a solution and reflects the effect of intermolecular interactions between the solute and solvent molecules. The activity coefficient is defined as the ratio of the actual activity a of a substance i in a solution to its ideal activity, which is equal to the mole fraction x of the substance.

$$\gamma_i = \frac{a_i}{x_i} \tag{2.14}$$

The activity coefficient can be calculated from the excess Gibbs energy G^E as follows [17]:

$$\ln \gamma_i = \left(\frac{\partial G^E / RT}{\partial n_i} \right)_{p,T,n_{j \neq i}} \tag{2.15}$$

The excess Gibbs energy describes the difference between the Gibbs energy of a real mixture and that of an ideal mixture of the same components. R is the universal gas constant, T the temperature and n the number of moles of component i.
As activity cofficient models describe systems at constant volume, they are not able to predict pressure and density.

2.6.2. Equations of state

Equations of states consist of an equation of states or a set of equations relating state variables of a given system in thermodynamic equilibrium. There is no universally valid equation of states that produces exact results for all substances under all conditions. Therefore, equations are defined in consonance with a thermodynamic model and their accuracy is limited. The equations are either derived from experimental data or based on physical and statistical considerations. The choice of the equation of state depends on the area of application and desired qualities, like the required accuracy, predictive ability, or the computational speed [18]. In the following, a few equations and the corresponding thermodynamic models will be illustrated.

The simplest example of an equation of state is the **ideal gas law** [19]:

$$p = \frac{RT}{v} \tag{2.16}$$

It relates the thermic values of state, temperature T, pressure p and molar volume v, of an ideal gas. The concept of an ideal gas is based on the physical model of its molecules as infinitely small, hard spheres which are moving in random directions. The particles do not interact with each other except through perfectly elastic collisions as there are no intermolecular forces or attractions between them. The molecules themselves take up zero volume. The ideal gas law cannot predict the behavior of liquids or phase transformations, as these occur due to intermolecular forces.
A real gas never behaves exactly like an ideal gas, but under conditions of low pressure and high temperatures, real gases approach the ideal state. Lower pressure means the distance between molecules is large and interactive forces reach a minimum. At higher temperatures, the kinetic energy of the molecules is higher and thereby, their ability to overcome intermolecular forces is higher. The deviation of the real gas' behavior from the ideal is reflected in the compressibility factor Z [6]:

$$Z = \frac{v_{real}}{v_{ideal}} \tag{2.17}$$

The compressibility factor of an ideal gas is 1. If $Z < 1$, the gas is compact and attractive forces between the molecules prevail. If $Z > 1$, the volume of the gas is bigger than the ideal volume and the molecules are repelling each other. The compressibility factors can be determined experimentally and are given as a function of pressure and temperature for many substances in the literature (e.g. [20]). The ideal gas law is then modified to reflect the behavior of real gases as follows:

$$p = \frac{ZRT}{v} \tag{2.18}$$

A well-used category of equations of state are **cubic equations of states**. They are derived semi-empirically and are characterized by a cubic polynomial function. The first of these equations was the **van der Waals equation** [6]. It is a modification of the ideal gas law and accounts for the deviation of real gases from ideal behavior by adding two corrective terms:

$$p = \frac{RT}{v - b} - \frac{a}{v^2} \tag{2.19}$$

The term $\frac{a}{v^2}$ accounts for the measured pressure being lower than predicted by the ideal gas law due to intermolecular attractive forces. The parameter b factors the finite

volume of real gas molecules, which reduces the volume of the gas and therefore the space for the motion of the molecules. This accounts for the repulsive forces, modeled as a one dimensional hard sphere repulsion. The van der Waals constants a and b are characteristics of a substance and calculated via its critical quantities. The equation is able to predict the p,V,T-behavior of liquid and gaseous phases, the process of liquification and vaporization as well as the equilibrium of liquids and vapor. However, the quantitative results show large deviations from measured values under conditions of low temperature and high pressure.
Other cubic equations of state are the **Soave-Redlich-Kwong equation** (equation 2.20) and the **Peng-Robinson equation** (equation 2.21) [21]. While the repulsive terms remain the same as in the van der Waals equation, the models provide two different modifications of the associative term. The model parameters a and b are fitted to experimental data or calculated using critical pressure and temperature.

$$p = \frac{RT}{v-b} - \frac{a(T)}{v(v+b)} \tag{2.20}$$

$$p = \frac{RT}{v-b} - \frac{a(T)}{v(v+b)+b(v-b)} \tag{2.21}$$

The equations are used for the calculation of thermodynamic behavior in the petroleum and chemical industries [21], as they can be applied over a wide range of pressures and temperatures and predict both liquid and vapor phases of substances such as hydrocarbons, in which dispersive and repulsive forces prevail.
In addition to ideal gas and cubic equations of state, there are other types of equations of state available, such as the **virial equations** [22], **Lennard-Jones Truncated and Shifted equations of state** (LJTS) [23], **Co-Oriented Fluid Functional Equation for Electrostatic interactions** (COFFEE) [24] or physically-based equations like the **Statistical Associating Fluid Theory** (SAFT) family [2]. These types of equations of state are typically formulated based on the Helmholtz energy. The model employed in this thesis is PC-SAFT, a widely used modification of SAFT.

2.6.3. Association models

Another category of models to predict thermodynamic properties are the so-called association models [21]. They were developed to describe the behavior of associating substances, such as water, alcohols and amines, which show great deviation from ideal behavior. Some association models are equations of state, however not all of them. Association models can be categorized in three groups:

- **Chemical theories** treat association like a chemical reaction and the associating

molecules as new and distinct chemical species [10]. The contribution of association to the total energy is related to the number of oligomers formed in the considered substance.

- In **Lattice Cluster Theory (LCT)**, fluids are modeled as having a lattice-like structure [10]. The extent of association is based on the number of hydrogen bonds formed between segments of molecules located on neighbouring sites in the lattice.
- In **perturbation theories**, the associative contribution is related to the number of bonding sites per molecule. To calculate the number of bonding sites, methods of statistical mechanics are applied. In mathematics, perturbation theory describes methods to find solutions for complex problems by adding corrective terms to a known solution for a related simpler problem [25].

While models of the first two groups are semi-empirical equations of state, perturbation theories are theoretically derived [11]. The PC-SAFT equation of state and the SAFT equation of state are both examples of perturbation theories. Therefore, the theoretical framework underlying this category will be elaborated in the upcoming chapters.

2.6.3.1. Perturbation Theory

SAFT and PC-SAFT are equations of state that belong to the category of perturbation theories. Perturbation theory is a mathematical method used to approximate the properties of a complex system by considering it as a perturbed version of a simpler system [26]. The starting point is a well-understood reference state, a solvable problem, which is then perturbed by adding small, incremental changes that make the problem more complex. The sought-after solution is calculated by expanding it in a power series of a small parameter that characterizes the perturbation. The first term in the series is the solution to the unperturbed problem, higher-order terms represent corrections due to the perturbation.

2.6.3.2. Wertheim's Thermodynamic Perturbation Theory

In thermodynamics, perturbation theories are used to approximate the thermodynamic properties of a fluid by relating it to a simple reference fluid. The target fluid's energy is described as the sum of the reference fluid's properties (e.g. expressed in terms of its Helmholtz energy) and perturbation or correction terms. The analytical equation for the target fluid is obtained by creating a Taylor expansion around the reference fluid [27]. This expansion converges quickly only when the structure of the reference fluid is similar to the target fluid's structure. Therefore, conventional perturbation theory cannot be applied to fluids in which strong associating forces are present [10]. In

Wertheim's thermodynamic perturbation theory [28][29][30][31] a multi-density formalism is introduced, in which the total number density can be written as the sum of the density of molecules present as monomers and the density of molecules bonded via association. In this notation, perturbation theory can be applied to any arbitrary reference fluid.
In Wertheim's contribution, all interactions between molecules are described by intermolecular potentials. A hard-sphere potential constitutes the reference potential, hence only representing the repulsive forces present between molecules. The molecule's ability to form associating bonds is modeled by introducing theoretical association sites on the molecule. The total intermolecular potential of the fluid $\Phi_{ij}(r)$is written as the sum of the intermolecular potential of the reference fluid $\Phi_{ij}^{ref}(r)$ and the sum of the potentials between the association site A on molecule i and association site B on molecule j $\Phi_{ij}^{AB}(r)$:

$$\Phi_{ij}(r) = \Phi_{ij}^{ref}(r) + \sum_{A}\sum_{B}\Phi_{ij}^{AB}(r) \tag{2.22}$$

The division of the pair potential into attractive and repulsive components enables the definition of the fluid's partition function, thereby facilitating the computation of its thermodynamic properties.

3. Theory

The following chapter provides a detailed overview of the Statistical Associating Fluid Theory (SAFT) and the Perturbed-Chain Statistical Associating Fluid Theory (PC-SAFT), including the underlying assumptions, equations, and applications. PC-SAFT is considered a variation of SAFT, the heterosegmental PC-SAFT uses the same set of equations as the original PC-SAFT, however modified to fit the heterosegmental depiction of molecules.

3.1. SAFT Equation of States

Wertheim's theory is the basis of SAFT, which was developed by Chapman et al. [2][32] and Huang and Radosz [33][34]. It is especially suited to describe the behavior of associating molecules with non-spherical shape, which are conceived as chains of spherical segments in the SAFT model. The SAFT equations of state are formulated in terms of the residual Helmholtz energy a_{res}, as properties like the pressure, compressibility factors and density can be derived from the Helmholtz energy. The residual Helmholtz energy describes the difference between the total Helmholtz energy a and the Helmholtz energy of an ideal gas a_{ideal} at the same pressure, temperature, and composition:

$$a_{res} = a - a_{ideal} \tag{3.1}$$

The reference fluid in SAFT equations is modeled differently in different versions of SAFT, e.g. by using a square-well potential [33] or Lennard-Jones [32] spheres. The residual Helmholtz energy of a real fluid a_{res} is given as the sum of the contributions due to different intermolecular forces (equation 3.2). a_{seg} describes the energy of segment-segment interactions (repulsion and dispersion), a_{chain} the energy due to chain formation and a_{assoc} the contribution due to association of the molecules. Further contributions can be added in a similar manner to model fluids that exhibit dipolar or quadrupolar interactions.

$$a_{res} = a_{seg} + a_{chain} + a_{assoc} + ... \tag{3.2}$$

The three major contributions to the total intermolecular potential of associating fluids according to SAFT are illustrated in figure 3.1. While the chain and the association term remain mostly unchanged [35], various modifications of the segment term have been proposed in variations of the SAFT model. These variations include for example simplified SAFT [36], the LJ–SAFT [37][38], the soft–SAFT [39][40], the SAFT–VR [41] and the PC–SAFT [1][42][43].

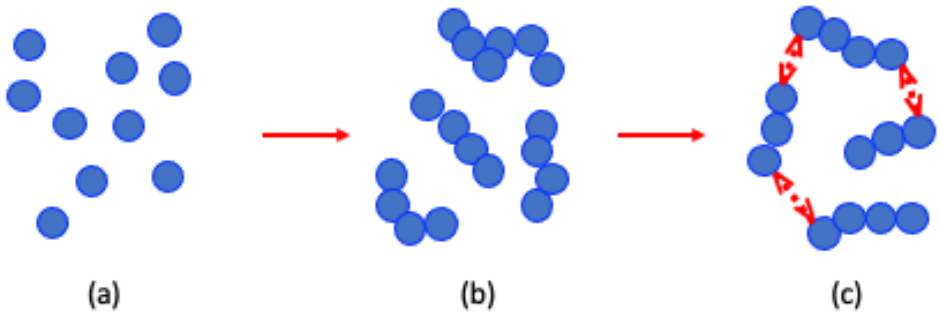

Figure 3.1.: Schematic representation of SAFT. Molecules are assumed to consist of equal-sized spherical segments (a), which are then connected to form chains (b). The ability to form hydrogen bonds (indicated by dotted arrows) is modeled by adding a certain number of association sites on the molecule (c).

In the following, the contributions to the total residual Helmholtz energy in equation 3.2 are illustrated according to Chapman et al. [32].

3.1.1. Segment contribution

The term a_{seg} in equation 3.2 refers to the Helmholtz energy per mole of molecules of spherical segments, which interact with repulsive and attractive dispersion forces. Physically, these segments correspond to a part of a complex molecule, a functional group, a monomer-section of a polymer or simple molecules like methane or argon [10]. The segment term is calculated as follows:

$$a^{seg} = a_0^{seg} \sum_i x_i m_i \tag{3.3}$$

a_0^{seg} is the segment molar Helmholtz energy per mole of segments, x_i the mole fraction, m_i the effective number of segments of molecule i. In the original SAFT model by Chapman et al. [32] the segments are defined to be Lennard-Jones spheres and their energy is composed of two parts:

$$a_0^{seg} = a_0^{hs} + a_0^{disp} \tag{3.4}$$

The term a_0^{hs} describes the energy of the reference fluid, a hard-sphere fluid, a_0^{disp} the dispersion or perturbation. The hard-sphere term is calculated according to Carnahan

and Sterling [44]:

$$\frac{a_0^{hs}}{RT} = \frac{4\eta - 3\eta^2}{(1-\eta)^2} \tag{3.5}$$

Here, η describes the packing fraction or reduced density.

$$\eta = \frac{\pi N_{Av}}{6} \rho d^3 \sum_i x_i m_i \tag{3.6}$$

The maximum packing fraction that can be achieved is 0.74, a value known as the close-packing limit or the densest packing fraction [45]. N_{Av} is Avogadro's constant. d is the temperature dependent segment diameter according to the theory of Barker and Henderson [25].

$$d(T) = \int_0^\sigma \left[1 - \exp\left(-\frac{\Phi(r)}{kT}\right)\right] dr \tag{3.7}$$

For mixtures, d is calculated by applying the van der Waals mixing rules.
In the SAFT model by Chapman et al. [32] the dispersion term a_0^{disp} is defined according to Cotterman et al. [46]

$$a_0^{disp} = \frac{\epsilon R}{k}\left(a_{01}^{disp} + \frac{a_{02}^{disp}}{T_R}\right) \tag{3.8}$$

Here, T_R is the reduced temperature

$$T_R = \frac{k_B T}{\epsilon} \tag{3.9}$$

ϵ is the characteristic energy of the system.

3.1.2. Chain contribution

In SAFT, the non-spherical molecular shape of the molecules is accounted for by chain formation. The formation of chains is modeled by placing association sites on the segments and strong interactions between them, representing the covalent bonds between atoms that form a molecule. Two diametrical sites enable the formation of chains, one site the formation of dimers. The calculation of the chain contribution to the total Helmholtz energy is given by:

$$\frac{a^{chain}}{RT} = \sum_i x_i (1 - m_i) \ln\left[g_{ii}(d_{ii})^{hs}\right] \tag{3.10}$$

$g_{ii}(d_{ii})^{hs}$ is the radial distribution function, which expresses the probability of finding a particle at a certain distance from a reference particle [47]. The radial distribution

function for hard spheres is derived by Reed and Gubbins [48] as:

$$g_{ij}(d_{ij})^{hs} = \frac{1}{1-\zeta_3} + \frac{3d_{ii}d_{jj}}{d_{ii}+d_{jj}}\frac{\zeta_2}{(1-\zeta_3)^2} + 2\left[\frac{d_{ii}d_{jj}}{d_{ii}+d_{jj}}\right]^2 \frac{(\zeta_2)^2}{(1-\zeta_3)^3} \tag{3.11}$$

ζ_k is a function of the density and is calculated as follows for $k = \{0, 1, 2, 3\}$:

$$\zeta_k = \frac{\pi N_{Av}}{6}\rho \sum_i x_i m_i d_{ii}^k \tag{3.12}$$

ζ_3 is equivalent to the packing fraction η given in equation 3.6.

3.1.3. Association contribution

In the SAFT model, as well as in Wertheim's original contribution, the molecules' ability to form associative bonds is modeled by placing association sites on the molecules. The associative interaction between two association sites is modeled with square-well potentials. Each molecule can contain multiple association sites. Due to the short-range and highly directional associative interactions, each association site is usually only singly bonded. In a "rigorous" definition, all electron-donor and -acceptor sites on a molecule are assigned association sites [33]. However, as the rigorous placement of association sites often does not lead to the most accurate results, alternative, arbitrary placements are defined which are then tested against experimental data and compared with the rigorous placement. In table 3.1 the rigorous placement of association sites, as well as one alternative placement, is illustrated for alkanols and water.

	Alkanols		**Water**	
	formula	bond type	formula	bond type
rigorous	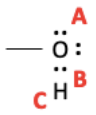	3B	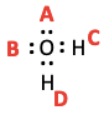	4C
alternative		2B	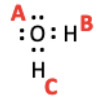	3B

Table 3.1.: Placement of association sites in alkanols and water [33]. The association sites are indicated by red, capital letters.

The association contribution is calculated as follows:

$$\frac{a^{assoc}}{RT} = \sum_i x_i \left[\sum_{A_i}\left(\ln X^{A_i} - \frac{X^{Ai}}{2}\right) + \frac{M_i}{2}\right] \tag{3.13}$$

where M_i is the number of bonding sites at component i, X^{A_i} the mole fraction of molecules of component i not bonded at association site A given by:

$$X^{A_i} = [1 + N_{Av} \sum_j \sum_{B_j} \rho_j X^{B_j} \Delta^{A_i B_j}]^{-1} \tag{3.14}$$

ρ_j is the molar density of the molecules of component j. The association strength $\Delta^{A_i B_j}$ between the bonding sites A and B on molecule i and j can be approximated as:

$$\Delta^{A_i B_j} = d_{ij}^3 g_{ij}(d_{ij})^{seg} \kappa^{A_i B_j} \left[\exp \frac{\epsilon^{A_i B_j}}{kT} - 1 \right] \tag{3.15}$$

$\kappa^{A_i B_j}$ describes the volume, $\epsilon^{A_i B_j}$ the energy of the association between association site A on component i and association site B on component j. The temperature dependent segment diameter d_{ij} corresponds to the arithmetic mean of diameter d_{ii} of molecule i and d_{jj} of molecule j.

$$d_{ij} = \frac{d_{ii} + d_{jj}}{2} \tag{3.16}$$

The segment radial distribution function $g_{ij}(d_{ij})^{seg}$ is approximated to be equal to the hard sphere radial distribution function $g_{ij}(d_{ij})^{hs}$ given in equation 3.11, as the segments are assumed as hard spheres.

In order to render equation 3.14 X^{A_i} explicit, a series of simplifying approximations can be made [33]. By assuming for example that the association strength between equal association sites is equal to zero and the strength of different hydrogen bonds is equivalent, the analytical expressions for X^{A_i} given in table 3.2 can be obtained for the types of bonds mentioned in table 3.1.

Bond type	**Δ approximations**	**X approximations**	**explicit X^A**
2B	$\Delta^{AA} = \Delta^{BB} = 0$ $\Delta^{AB} \neq 0$	$X^A = X^B$	$\frac{-1+(1+4\rho\Delta)^{1/2}}{2\rho\Delta}$
3B	$\Delta^{AA} = \Delta^{AB} = \Delta^{BB} = \Delta^{CC} = 0$ $\Delta^{AC} = \Delta^{BC} \neq 0$	$X^A = X^B$ $X^C = 2X^A - 1$	$\frac{-(1-\rho\Delta)+((1+\rho\Delta)^2+4\rho\Delta)^{1/2}}{4\rho\Delta}$
4C	$\Delta^{AA} = \Delta^{AB} = \Delta^{BB} = \Delta^{CC} = \Delta^{CD} = \Delta^{DD} = 0$ $\Delta^{AC} = \Delta^{AD}\Delta^{BC} = \Delta^{BD} \neq 0$	$X^A = X^B = X^C = X^D$	$\frac{-1+(1+8\rho\Delta)^{1/2}}{4\rho\Delta}$

Table 3.2.: Simplified approximations for association strengths Δ between association sites and explicit equations for the mole fraction X not bonded at the association site according to [33].

3.1.4. SAFT parameters

In the SAFT model each component is characterized by five pure parameters, which are given in table 3.3. In most versions of SAFT models, the parameters are obtained by fitting them to experimental data of the pure compounds, like vapor pressure and saturated liquid density.

SAFT parameter	
m_i	number of segments of component i
σ_i	diameter of segment of component i
ϵ_i	energy of segment of component i
$\kappa_{A_iB_j}$	association volume between association site A on component i and association site B on component j
$\epsilon_{A_iB_j}$	association energy between association site A on component i and association site B on component j

Table 3.3.: The molecule specific parameters used in SAFT equations of states.

3.2. PC-SAFT Equation of States

The Perturbed-Chain Statistical Association Fluid Theory, short PC-SAFT, is a modification of SAFT, developed by Gross and Sadowski [1][42][43]. Instead of hard-spheres, PC-SAFT uses a hard-chain fluid as reference fluid for the perturbation. The dispersion potential is added between the connected segments instead of between segments. Like the SAFT equation of state, PC-SAFT equation of state is formulated in terms of residual Helmholtz energy. The perturbation terms, which are added to the energy of the reference fluid a_{hc}, are the dispersion energy a_{disp}, and the energy due to association a_{assoc} for associating substances. Later, the theory was expanded to describe quadrupolar interaction by adding the quadrupole contribution a_{quad} [49]. Further terms, for example to model dipolar contributions, can be added in a similar matter.

$$a_{res} = a_{hc} + a_{disp} + a_{assoc} + a_{quad} + ... \tag{3.17}$$

In the following, the equations to calculate the amount of each contribution to the total residual Helmholtz energy of the fluid are illustrated in the notation of [1][42][43].

3.2.1. Chain contribution

The pair potentials of the individual segments which comprise a chain are modeled with a modified square-well potential [50]:

$$\Phi_{ij}(r) = \begin{cases} 0 & \text{if} \quad r \geq \lambda\sigma \\ -\epsilon & \text{if} \quad \sigma \leq r < \lambda\sigma \\ 3\epsilon & \text{if} \quad (\sigma - s_1) \leq r < \sigma \\ \infty & \text{if} \quad r < (\sigma - s_1) \end{cases} \tag{3.18}$$

In comparison to the square-well potential given in equation 2.13, in the modified square-well potential a repulsion energy 3ϵ is added at radial distances r that lie between the diameter σ and $\sigma - s_1$. Gross and Sadowski [1] assume, in accordance with Chen and Kreglewski [50], a s_1/σ ratio of 0.12. λ factors the well width. The step function approximates a soft repulsion (see figure 2.3b). The resulting modified square-well potential is illustrated in figure 3.2.

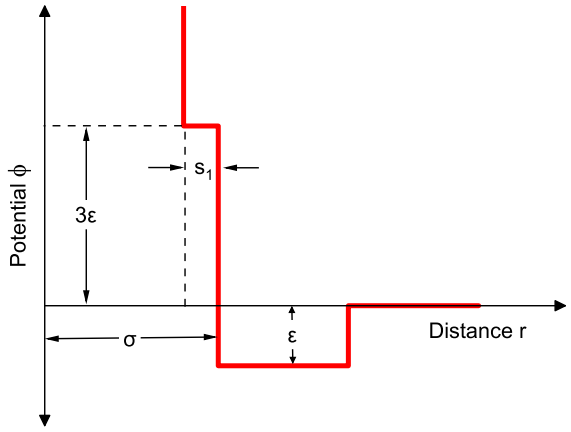

Figure 3.2.: Modified square-well potential according to [50] used in the PC-SAFT equations of state [1].

The reference fluid in PC-SAFT is a hard-chain fluid, constituting the repulsive interactions of the molecules. The segments of a chain interact with hard repulsion, their diameter d is calculated temperature-dependent (see equation 3.7). For the potential given in equation 3.18, the diameter is calculated as follows:

$$d_i(T) = \sigma_i \left[1 - 0.12 \exp\left(-\frac{3\epsilon_i}{kT}\right)\right] \tag{3.19}$$

The hard-chain term (equation 3.20) is formulated analog to the hard-chain term in SAFT equations (equation 3.10).

$$\tilde{a}^{hc} = \bar{m}\tilde{a}^{hs} - \sum_i x_i(1-m_i)\ln\left[g_{ii}(d_{ii})\right] \tag{3.20}$$

In the notation of Gross et al. the tilde indicates reduced properties which are obtained by normalizing a given variable with respect to the Boltzmann's constant and the temperature as illustrated in equation 3.21.

$$\tilde{a} = \frac{a}{k_B T} \tag{3.21}$$

The mean segment number $\bar{m}$ of the mixture is:

$$\bar{m} = \sum_i x_i m_i \tag{3.22}$$

The Helmholtz energy of the segment $\tilde{a}^{hs}$ is calculated as follows:

$$\tilde{a}^{hs} = \frac{1}{\zeta_0}\left[\frac{3\zeta_1\zeta_2}{(1-\zeta_3)} + \frac{(\zeta_2)^3}{\zeta_3(1-\zeta_3)^2} + \left(\frac{(\zeta_2)^3}{(\zeta_3)^2} - \zeta_0\right)\ln(1-\zeta_3)\right] \tag{3.23}$$

The calculation of ζ_k is given in equation 3.12.

3.2.2. Dispersion contribution

Within the PC-SAFT framework, the second order perturbation theory of Barker and Henderson [25][51] is applied to calculate the attractive part of the chain interactions, the contribution to the residual Helmholtz energy due to dispersion $\tilde{a}^{disp}$ (equation 3.24). The theory was originally derived for spherical segments and is extended to chain molecules by adding up the individual segment-segment interactions between chain molecules.

$$\begin{aligned}\tilde{a}^{disp} = &-2\pi\rho I_1(\bar{m},\eta)\sum_i\sum_j x_i x_j m_i m_j\left(\frac{\epsilon_{ij}}{kT}\right)\sigma_{ij}^3 - \\ &\pi\rho\bar{m}\left(1 + Z^{hc} + \rho\frac{\partial Z^{hc}}{\partial\rho}\right)^{-1} I_2(\bar{m},\eta)\sum_i\sum_j x_i x_j m_i m_j\left(\frac{\epsilon_{ij}}{kT}\right)^2\sigma_{ij}^3\end{aligned} \tag{3.24}$$

In order to solve the functions I_1 (equation 3.25) and I_2 (equation 3.26), universal model constants (equations 3.27 and 3.28) are fitted to experimental pure component data of the series of n-alkanes. The values of these constants are given in [1]. The dependence of the coefficients $a_i(\bar{m})$ and $b_i(\bar{m})$ on the segment number (equations 3.27 and 3.28) has

been derived by Liu and Hu [52].

$$I_1(\eta, \bar{m}) = \sum_{i=0}^{6} a_i(\bar{m})\eta^i \tag{3.25}$$

$$I_2(\eta, \bar{m}) = \sum_{i=0}^{6} b_i(\bar{m})\eta^i \tag{3.26}$$

$$a_i(\bar{m}) = a_{0i} + \frac{\bar{m}-1}{\bar{m}}a_{1i} + \frac{\bar{m}-1}{\bar{m}}\frac{\bar{m}-2}{\bar{m}}a_{2i} \tag{3.27}$$

$$b_i(\bar{m}) = b_{0i} + \frac{\bar{m}-1}{\bar{m}}b_{1i} + \frac{\bar{m}-1}{\bar{m}}\frac{\bar{m}-2}{\bar{m}}b_{2i} \tag{3.28}$$

3.2.3. Association contribution

In PC-SAFT, the association contribution is calculated exactly like the association contribution introduced in chapter 3.1.3. The reduced Helmholtz energy due to association in the fluid is given by:

$$\tilde{a}^{assoc} = \sum_i x_i \left[\sum_{A_i} \left(\ln X^{A_i} - \frac{X^{A_i}}{2} \right) + \frac{M_i}{2} \right] \tag{3.29}$$

3.2.4. Quadrupole contribution

The contribution to the total Helmholtz energy due to quadrupole-quadrupole interactions is defined in a later publication by Gross [49] as

$$\tilde{a}^{quad} = \frac{\tilde{a}_2}{1 - \tilde{a}_3/\tilde{a}_2} \tag{3.30}$$

Here, $\tilde{a}_2$ and $\tilde{a}_3$ are the second and third order perturbation terms to the reference fluid, which are given as:

$$\tilde{a}_2 = -\pi \left(\frac{3}{4}\right)^2 \rho \sum_i \sum_j x_i x_j \frac{\epsilon_{ii}}{k_B T}\frac{\epsilon_{jj}}{k_B T}\frac{\sigma_{ii}^5 \sigma_{jj}^5}{\sigma_{ij}^7} n_{Q,i} n_{Q,j} {Q^*}_i^2 {Q^*}_j^2 J_{2,ij} \tag{3.31}$$

$$\begin{aligned}\tilde{a}_3 = {} & \frac{\pi}{3}\left(\frac{3}{4}\right)^3 \rho \sum_i \sum_j x_i x_j \left(\frac{\epsilon_{ii}}{k_B T}\right)^{3/2}\left(\frac{\epsilon_{jj}}{k_B T}\right)^{3/2}\frac{\sigma_{ii}^{15/2}\sigma_{jj}^{15/2}}{\sigma_{ij}^{12}} \\ & \times n_{Q,i} n_{Q,j} Q_i^{*3} Q_j^{*3} J_{3,ij} + \frac{4\pi^2}{3}\left(\frac{3}{4}\right)^3 \rho^2 \sum_i \sum_j \sum_k x_i x_j x_k \\ & \times \frac{\epsilon_{ii}}{k_B T}\frac{\epsilon_{jj}}{k_B T}\frac{\epsilon_{kk}}{k_B T}\frac{\sigma_{ii}^5 \sigma_{jj}^5 \sigma_{kk}^5}{\sigma_{ij}^3 \sigma_{ik}^3 \sigma_{jk}^3} n_{Q,i} n_{Q,j} n_{Q,k} {Q^*}_i^2 {Q^*}_j^2 {Q^*}_k^2 J_{3,ijk}\end{aligned} \tag{3.32}$$

n_Q is the number of quadrupolar moments per molecules of component i. ${Q^*}_i^2$ is the squared dimensionless quadrupolar moment, calculated from the squared quadrupolar moment Q_i^2 as follows:

$${Q^*}_i^2 = \frac{Q_i^2}{m_i \epsilon_{ii} \sigma_{ii}^5} \tag{3.33}$$

To solve the functions $J_{2,ij}$, $J_{3,ij}$ and $J_{3,ijk}$ (equations 3.34, 3.35 and 3.36), the model constants $a_{0,n}$, $b_{0,n}$, $c_{0,n}$, $a_{1,n}$, $a_{2,n}$, $b_{1,n}$, $b_{2,n}$, $c_{1,n}$ and $c_{2,n}$ are adjusted to simulation data.

$$J_{2,ij} = \sum_{n=0}^{4} \left(a_{n,ij} + b_{n,ij} \frac{\epsilon_{ij}}{k_B T} \right) \eta^n \tag{3.34}$$

$$J_{3,ijk} = \sum_{n=0}^{4} c_{n,ijk} \eta^n \tag{3.35}$$

$$J_{3,ij} = 0 \tag{3.36}$$

$$a_{n,ij} = a_{0n} + \frac{m_{ij}-1}{m_{ij}} a_{1n} + \frac{m_{ij}-1}{m_{ij}} \frac{m_{ij}-2}{m_{ij}} a_{2n} \tag{3.37}$$

$$b_{n,ij} = b_{0n} + \frac{m_{ij}-1}{m_{ij}} b_{1n} + \frac{m_{ij}-1}{m_{ij}} \frac{m_{ij}-2}{m_{ij}} b_{2n} \tag{3.38}$$

$$c_{n,ijk} = c_{0n} + \frac{m_{ijk}-1}{m_{ijk}} c_{1n} + \frac{m_{ijk}-1}{m_{ijk}} \frac{m_{ijk}-2}{m_{ijk}} c_{2n} \tag{3.39}$$

The dependence of the constants on the chain length was derived by Hu et al.[53][52]. m_{ij} and m_{ijk} are obtained from the chain length parameters with the following combining rules:

$$m_{ij} = (m_i m_j)^{1/2} \tag{3.40}$$

$$m_{ijk} = (m_i m_j m_k)^{1/3} \tag{3.41}$$

3.2.5. PC-SAFT parameters

The nomenclature of the parameters in the PC-SAFT equations remains the same as given for SAFT in table 3.3. However, due to differences in the equations, the parameter values for a given substance are not the same. Gross et al. [1][42] obtained the parameters by fitting them to pure-component data for different fluids such as alkanes, alkenes, aromatics, chlorinated hydrocarbons, ethers and esters. For systems which consist of two or more components, the parameters of unlike segments are determined by applying the Berthelot-Lorentz combining rules [54] (see equations 3.42 and 3.43). Unlike segments are for example considered in the calculation of the dispersion energy in equation 3.24.

$$\sigma_{ij} = \frac{1}{2}(\sigma_i + \sigma_j) \tag{3.42}$$

$$\epsilon_{ij} = \sqrt{\epsilon_i \epsilon_j}(1 - k_{ij}) \tag{3.43}$$

Here, a correction term is introduced in the form of the binary interaction parameter k_{ij}. This correction term can be defined to be a constant for a specific mixture of component i and j, temperature dependent or dependent on the concentration.

3.3. Heterosegmental PC-SAFT equation of state

In order to model polymers, Gross et al. extended the PC-SAFT model to describe heterosegmental molecules [3]. While homopolymers are composed of a single repeating monomer type, copolymers consist of two or more monomers arranged in repeat units [55]. The sequence of these repeat units is random in many technical copolymers. In comparison to the homosegmental approach, where molecules are considered to consist of equal-sized identical spheres, the heterosegmental approach allows the division of molecules into different segments, reflecting the different components of copolymers. Figure 3.3 shows a copolymer molecule comprised of two different segments.
Each type of segments is characterized by a set of parameters (table 3.5) which are the same as in the SAFT model. In contrast to SAFT and PC-SAFT however, these parameters are not defined for a specific molecule but for one type of segments.
The order of the spheres within the polymer chain is not considered in the approach.

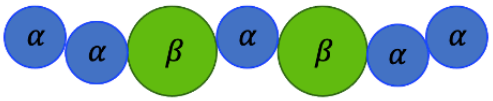

Figure 3.3.: Schematic representation of a copolymer in the heterosegmental PC-SAFT approach of Gross et al. [3]. Spheres of different segments are indicated by α and β.

The composition of different segments is reflected by introducing the segment fraction $z_{i\alpha}$ and the bonding fraction $B_{i\alpha i\beta}$. The letter i indicates the component, the greek letter subscripts the segment. Equation 3.44 shows the calculation of the segment fraction.

$$z_{i\alpha} = \frac{m_{i\alpha}}{m_i} \tag{3.44}$$

The calculation of the bonding fraction between segment α and β according to Gross et al. [3] depends on the repeat unit composition and is given in table 3.4a. Haarmann et al. [57][56] applied the heterosegmental model to polar and associating long-chain molecules, e.g. methyl alkanoates and alcohols. These molecules consist of a functional head moiety and n-alkylic residues, modeled as "head" and "tail" segments of the molecule (see figure 3.4). Due to the known sequence of segments in this approach, the bonding fraction is

		$B_{i\alpha i\beta}$	$B_{i\alpha i\alpha}$	$B_{i\beta i\beta}$		B_{iTiT}	B_{iHiH}	B_{iTiH}
(a)	$z_{i\beta} < z_{i\alpha}$	$2\frac{z_{i\alpha}m_i}{m_i-1}$	$1 - B_{i\alpha i\beta} - B_{i\beta i\alpha}$	0	(b)	$\frac{m_{iT}-1}{m_i-1}$	$\frac{m_{iH}-1}{m_i-1}$	$\frac{1}{m_i-1}$
	$z_{i\beta} > z_{i\alpha}$	$2\frac{z_{i\beta}m_i}{m_i-1}$	0	$1 - B_{i\alpha i\beta} - B_{i\beta i\alpha}$				
	$z_{i\beta} = z_{i\alpha}$	1	0	0				

Table 3.4.: (a) Calculation of the bonding fraction in PC-SAFT approach according to Gross and Sadowski [3]. (b) Calculation of the bonding fraction in PC-SAFT approach according to Haarmann et al. [56].

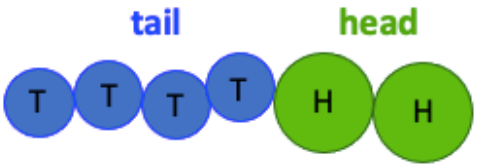

Figure 3.4.: Schematic representation of a molecule in the heterosegmental PC-SAFT approach of Haarmann et al. [57][56]. A molecule with tail segment and head segment.

calculated as given in table 3.4b. The subscripts T and H indicate the tail and head segment and replace tha α and β subscripts of Gross et al. [3]. The head segment in Haarmann's model consists of what is known as the functional group in organic chemistry plus the first adjacent carbon atom of the alkyl residue and its hydrogen atoms. A pentanol molecule for example is divided into two segments. The head segment is the hydroxyl functional group plus the first carbon atom and its hydrogen atoms ($-CH_2OH$). The alkyl residue for pentanol is a butyl residue ($-C_4H_7$). The structure of n-pentanol in the heterosegmental approach is shown schematically in figure 3.5.

The chain, dispersion, association and quadrupole contributions to the total Helmholtz

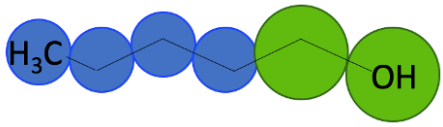

Figure 3.5.: Schematic representation of the molecule n-pentanol in the heterosegmental PC-SAFT approach.

energy of the fluid are calculated analog to the original PC-SAFT. The respective equations in the notation of the heterosegmental PC-SAFT can be found in the appendix.

3.3.1. Heterosegmental PC-SAFT parameters

The model parameters used in the heterosegmental PC-SAFT equations of states remain the same as in the previously discussed SAFT and the homosegmental PC-SAFT. However,

the parameters have to be defined for each type of segments of a molecule. Gross et al.

Heterosegmental PC-SAFT parameter	
$m_{i\alpha}$	segment number of segment-type α of component i
$\sigma_{i\alpha}$	segment diameter of segment-type α of component i
$\epsilon_{i\alpha}$	segment energy of segment-type α of component i
$\kappa_{A_{i\alpha}B_{j\beta}}$	association volume between association site A on segment-type α of component i and association site B on segment-type β of component j
$\epsilon_{A_{i\alpha}B_{j\beta}}$	association energy between association site A on segment-type α of component i and association site B on segment-type β of component j

Table 3.5.: The parameters used in the heterosegmental PC-SAFT equations of states. In the notation of Haarmann et al. [57][56] α and β is replaced by T and H (head and tail segment)

[3] apply the heterosegmental model to copolymers. For a copolymer consisting of joined n-alkanes, each part of the molecule or segment type is assigned the parameters of the corresponding pure component homosegmental n-alkane.
Haarmann et al. [57][56] modify the heterosegmental model to describe molecules comprised of head and tail segments. The tail segment is the alkyl-residue of the molecule. It is modeled with the parameters of the corresponding n-alkane. The parameters for the head segment, e.g. the primary-alcohol domain ($-CH_2OH$), the primary-amine domain ($-CH_2NH_2$), and the carboxylic-acid domain ($-COOH$), are then fitted to the vapor-pressure data and saturated liquid-density data of n-octanol, n-octyl amine, and n-octanoic acid respectively.
The binary dispersive interaction parameter (see equation 3.43) can be applied for each individual segment-segment interaction.

4. Implementation of the Heterosegmental PC-SAFT Model

The heterosegmental PC-SAFT equations are used to predict thermodynamic properties of systems in thermodynamic eqilibrium. The equilibrium conditions employed in the implementation of the model are the equality of chemical potential for each substance in all phases and the equality of pressure in all phases. The present work focuses on vapor-liquid equilibria for pure and binary systems.
The workflow of the implemented model is illustrated in figure 4.1 and 4.2. For pure systems (figure 4.1), the method calculates the pressure-temperature relationship for the substance in question, while for binary systems (figure 4.2), the pressure-composition relationship is calculated at a specific temperature. In both methods, the volume is constant.

4.1. Pure systems

For pure systems, the model conducts iterative calculations over a range of temperatures. Prior to the iteration process, it is necessary to define the initial temperature and the corresponding liquid density. An initial value for the vapor pressure is calculated with the Wagner equation, then, the initial density of the vapor phase is calculated as a function of the obtained initial pressure.
The initial values are passed to a solver to calculate the density, the compressibility factor, the chemical potential and the pressure for the vapor and liquid phase at equilibrium conditions. At equilibrium conditions the differences between the chemical potential in the liquid and vapor phase and the pressure in the liquid and vapor phase reach a minimum. The solver algorithm is based on the Powell's method. The obtained values are then used as initial values for the next temperature step. The calculation terminates, when the set maximum iteration steps are reached or when the densities of the vapor and liquid phase become indistinguishable, signifying that the critical point has been reached.

4.2. Binary sytems

For binary systems, the model iterates over the composition of the liquid phase at a set temperature, commencing from a liquid mole fraction x_{liquid} of the light volatile

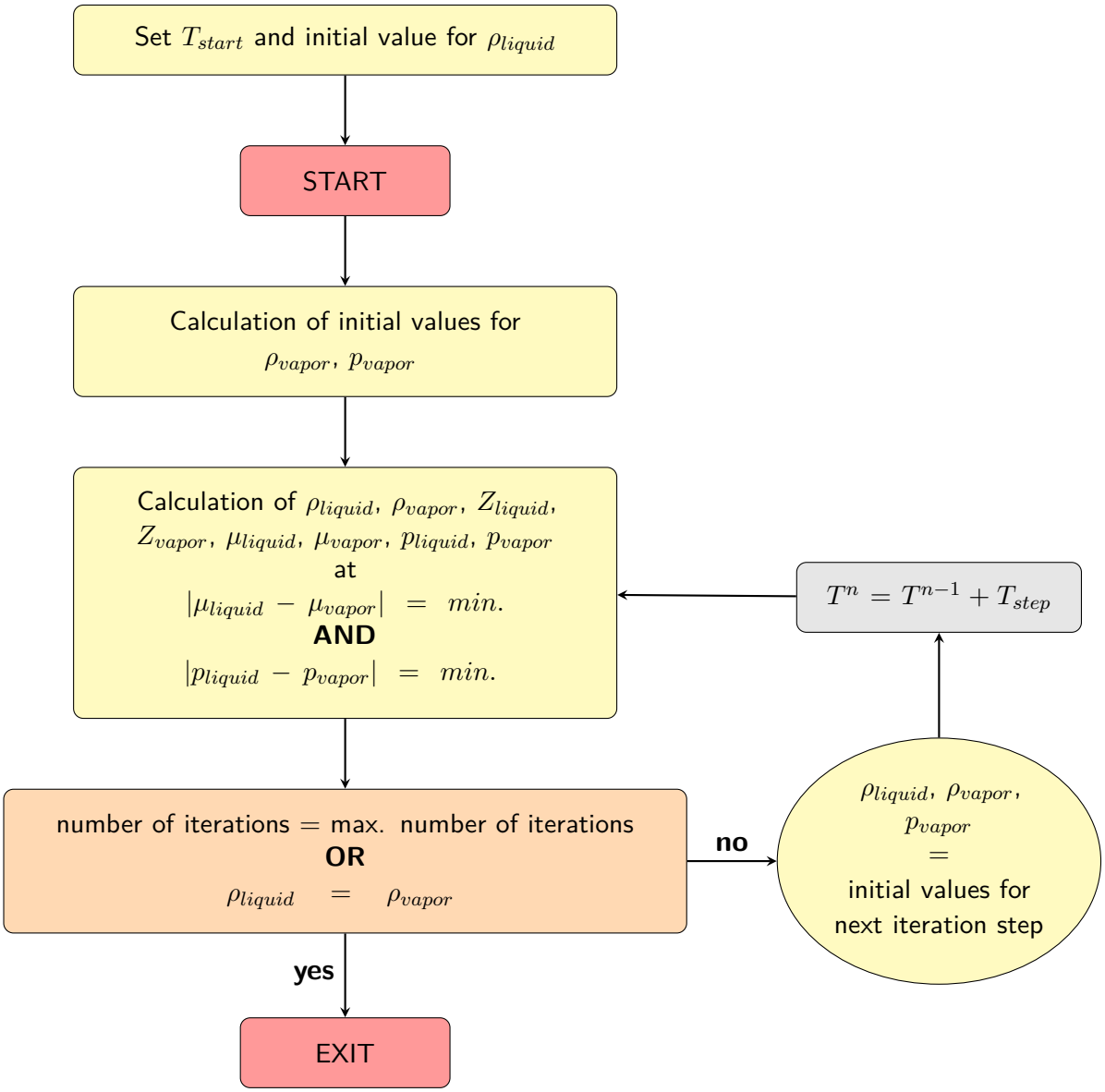

Figure 4.1.: Flow diagram of the implemented PC-SAFT model for pure systems. The calculation of thermodynamic properties is iterated over temperature.

component of 0 and advancing towards 1. The initial values are the same as for pure systems. For the first iteration step, where the percentage of the light volatile component is zero, the method for pure systems is applied to calculate the vapor pressure, liquid and vapor densities for the second component at the set temperature. The obtained values serve as the initial values for the next iteration, where the liquid mole fraction of the first component is incremented by the specified step size. In each step, the Powell solver calculates the compressibility factor, the density and the pressure for both the vapor and the liquid phase, the chemical potential for each component in the vapor and the liquid phase, as well as the vapor mole fraction of the volatile component at equilibrium conditions. The calculation is terminated when the maximum iteration steps are reached, when the liquid mole fraction of the volatile component reaches 1, or when the system reaches its critical point.

4.3. Average relative deviation (ARD)

The evaluation of the results was performed by calculating the percentage average relative deviation (%ARD). ARD is a statistical measure commonly used to evaluate the agreement between two sets of data, such as simulation results and experimental measurements. The %ARD formula can be expressed mathematically as:

$$\%\mathrm{ARD} = \frac{1}{N_{\mathrm{data}}} \sum_{i=1}^{N_{\mathrm{data}}} \left| 1 - \frac{f_d^{\mathrm{set1}}}{f_d^{\mathrm{set2}}} \right| 100\% \tag{4.1}$$

where f_d^{set1} and f_d^{set2} represent the data points of the compared data sets (e.g. experimental and model data), and N_{data} is the total number of data points. The resulting value of %ARD provides an indication of the average percentage deviation between the two sets of data, with lower values indicating better agreement.
To discuss pure systems, the %ARD is calculated as the deviation between the experimental vapor pressure and the modeled pressure at the same temperature. For binary systems two different %ARDs are defined. $\%\mathrm{ARD}_{\Delta p}$ gives the deviation of experimental and modeled vapor pressure at the same liquid mole fraction of the volatile component, $\%\mathrm{ARD}_{\Delta y}$ is the deviation of the respective vapor mole fraction of the volatile component at the same liquid composition.

4.4. Fitting of the binary correction parameters

The binary parameter k_{ij} is used to correct the dispersive cross-interaction between two substances in the PC-SAFT equations (cf. equation 3.24 and A.3).

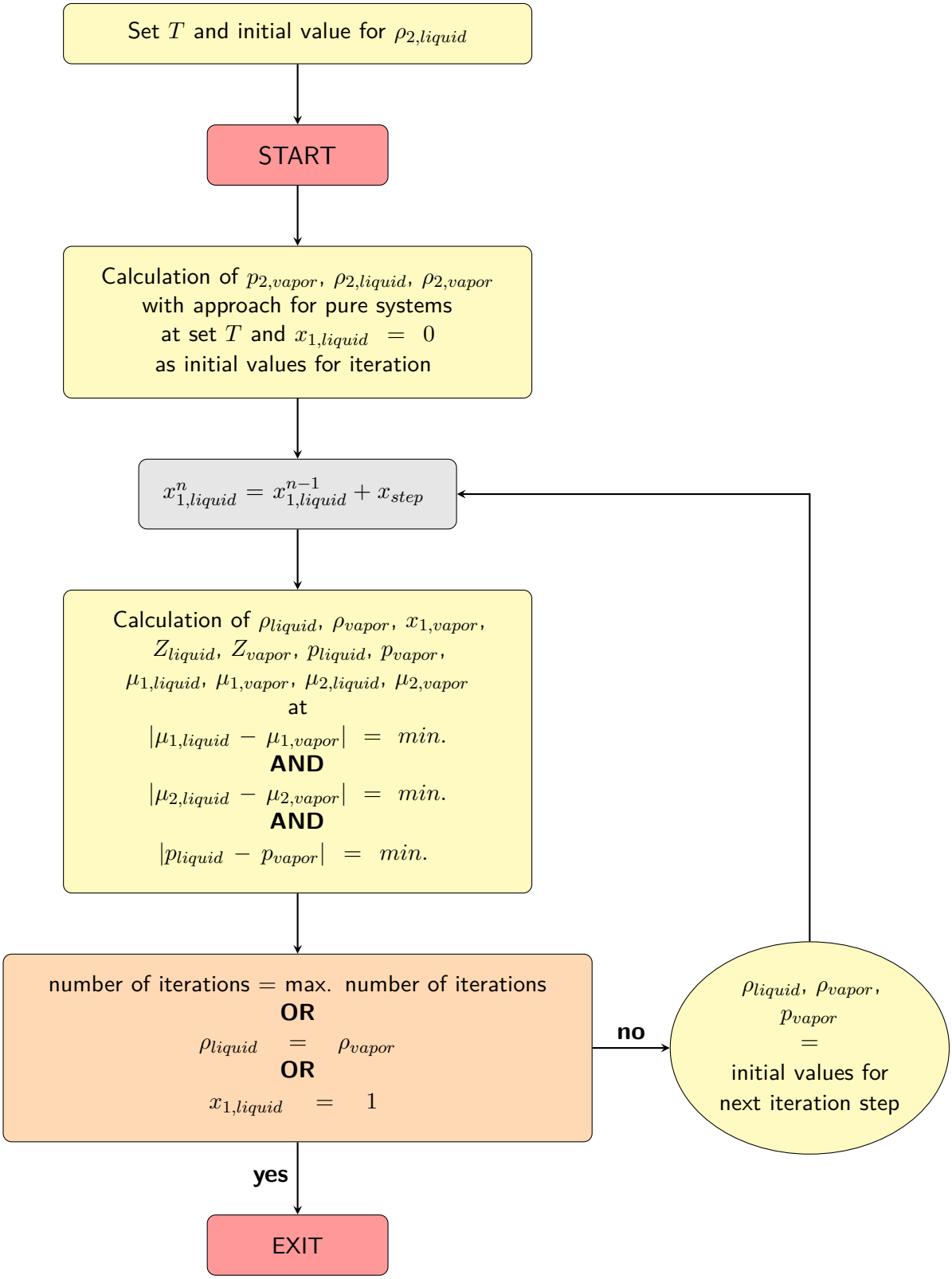

Figure 4.2.: Flow diagram of the implemented PC-SAFT model for binary systems consisting of component 1 and component 2. The calculation of thermodynamic properties is iterated over the liquid mole fraction of component 1 at a set temperature.

In the present work the binary parameters between alkanes and the alkyl-residue of alcohols were set to zero, due to their similarity. In accordance with Haarmann et al. [56] the binary parameter between the head moiety of alcohols and alkanes was set to zero to keep the predictive ability of the model.
To model binary alcohol - CO_2 systems with the heterosegmental PC-SAFT approach two binary parameters are defined which correct the alkyl residue - CO_2 interaction and the ($-CH_2OH$) - CO_2 interaction as illustrated in figure 4.3. The alkyl residue - CO_2

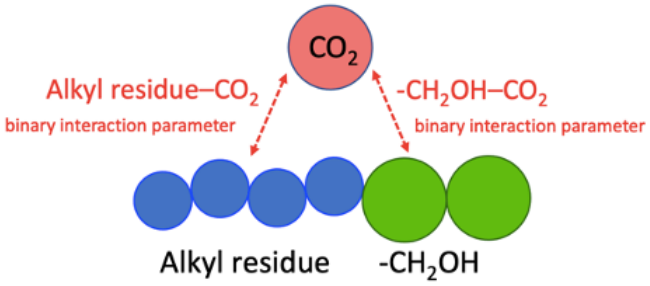

Figure 4.3.: Schematic illustration of the binary parameters used to correct the alkyl residue CO_2 interaction and the ($-CH_2OH$)-CO_2 interaction between the head segment of the alcohol molecule and CO_2 in the heterosegmental PC-SAFT approach.

parameters were assumed to be consistent with the respective homosegmental alkane - CO_2 parameters. Perez et al. [58] established that the values of the binary parameter for the n-alkane - CO_2 interaction fluctuate around a mean value, independent of the number of C-atoms and the temperature. However, the authors did not consider quadrupole interactions in their simulation, hence the tabulated binary parameters can not be used to correct the interactions in simulations considering quadrupole moments.
To obtain the alkane - CO_2 binary parameters pertinent to this thesis, the binary parameters of CO_2 - propane, CO_2 - heptane and CO_2 - dodecane systems were fitted to experimental data. The binary parameters and the computed mean value are given in table 4.1. The alkane - CO_2 interaction parameter is assumed to be a constant and independent of the temperature and the number of C-atoms.
Then, the binary parameter for the ($-CH_2OH$) - CO_2 interaction was adjusted to the CO_2 - octanol system at different temperatures, while the alkyl residue - CO_2 binary parameter was set to $k_{ij} = 0.04$ (see table 4.1). This is in accordance with the approach of Haarmann et al.[57][56], who obtained the PC-SAFT parameters of the head segments by fitting them to experimental data of n-octanol, n-octyl amine, and n-octanoic acid. As shown in figure 4.4, for higher pressures and CO_2-concentrations the curve shows great deviation from the experimental results. For this reason, the binary parameters were fitted to experimental data points of the bubble point curve up to 40 % of the maximum

Binary system	**Temperature**	k_{ij}
CO_2 - Propane	277.59 K	0.04
CO_2 - Heptane	310.64 K	0.03
CO_2 - Dodecane	417.91 K	0.05
Mean value	-	0.04

Table 4.1.: Binary parameters fitted for the systems CO_2 - propane, CO_2 - heptane and CO_2 - dodecane at given T. The mean value is used as a constant to model the binary alkyl residue - CO_2 parameter in alcohol - CO_2 systems.

experimental pressure of the data. The fitting process was performed using the ARD method, minimizing the error between the modeled vapor pressure and the experimental vapor pressure at the same liquid composition. The binary parameter for the ($-CH_2OH$)

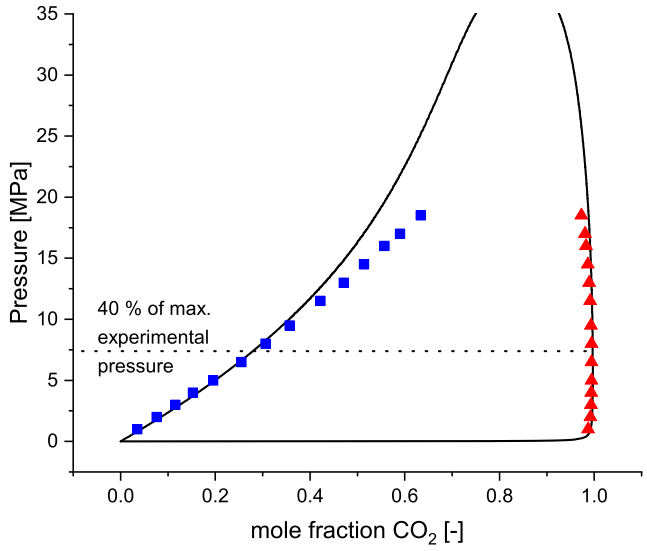

Figure 4.4.: The model results for the CO_2 - octanol system at T = 403.15 K are plotted against experimental data [59] (bubble point curve: blue squares; dew curve: red triangles). A dashed line indicates 40% of the maximum pressure of the experimental data. Only data points below this line were considered in the fitting process of the binary ($-CH_2OH$) - CO_2 parameter.

- CO_2 interaction as a function of the temperature is illustrated in figure 4.5. A line of best fit shows the binary parameter as a function of temperature is approximately linear. The obtained temperature-dependent binary parameter was then used to model the alcohol - CO_2 systems shown in chapter 5.

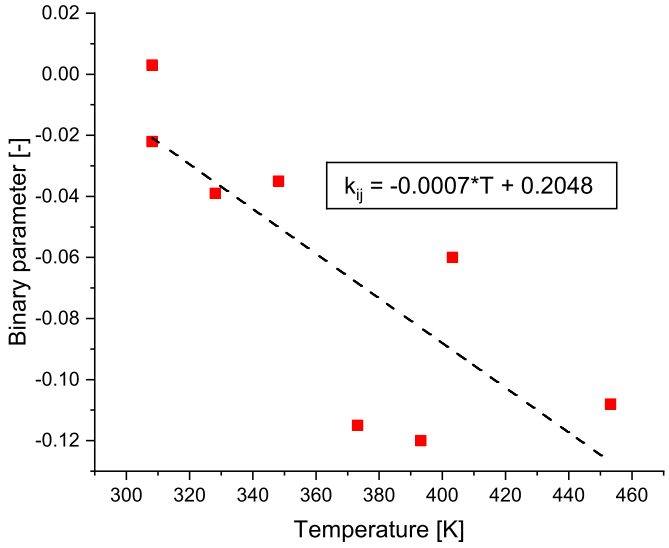

Figure 4.5.: The binary parameter for the ($-CH_2OH$) - CO_2 interaction as a function of temperature. Fitted for CO_2 - octanol systems below 40% of the maximum experimental pressure. The binary parameter between the alkyl residue and CO_2 is k_{ij}=0.04.

5. Results and Discussion

The implementation of the model was validated by applying it to the same systems modeled by Haarmann et al. [56], who implemented the heterosegmental PC-SAFT approach for associating systems. The model was first assessed for pure and binary associating systems and then applied to predict the behavior of three different binary butane - alcohol systems at two different temperatures.
Then, the model was expanded to incorporate a quadrupolar interaction term based on Gross [49]. The term was modified to be consistent with the heterosegmental PC-SAFT approach and applied in the modeling of binary CO_2 - alcohol systems. The simulation results were compared to experimental data in terms of their average relative deviation. Additionally, the results of the heterosegmental approach were compared to the homosegmental approach to assess if the inclusion of a second binary parameter can enhance the model's ability to accurately predict the behavior of binary CO_2 - alcohol systems.

5.1. Validation of the model implementation

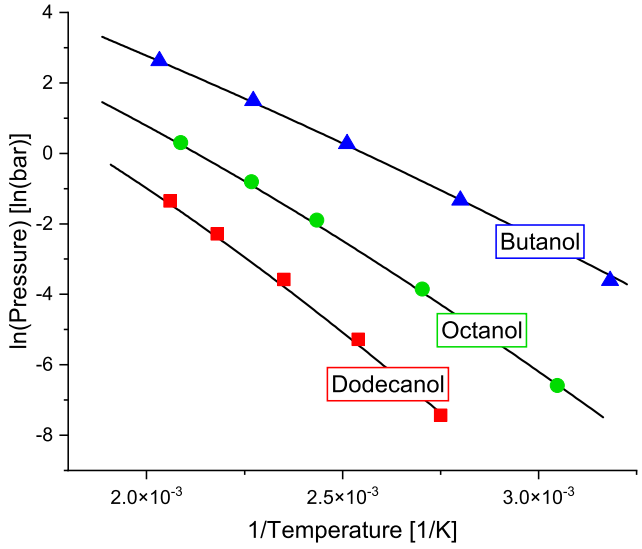

Figure 5.1.: Logarithm of pure-component vapor pressure as a function of the inverse temperature for n-butanol, n-octanol and n-dodecanol. Solid lines show the model results, symbols the experimental data. References are given in table 5.1.

System	N_{data}	$\%ARD$	references
n-Butanol	5	5.21	[60][61][62][63][64]
n-Octanol	5	7.37	[65][66][67][68][69]
n-Dodecanol	5	11.64	[70][71][72][73][74]

Table 5.1.: %ARD values for the model predictions for pure systems (figure 5.1). References for experimental data points are given in ascending order of T, N_{data} indicates the number of data points.

	System	Temperature	N_{data}	$\%ARD_{\Delta p}$	$\%ARD_{\Delta y}$	ref
(a)	Butane and Butanol	364.5 K	26	4.13	0.95	[75]
(b)	Undecane and Butanol	373.12 K	15	4.8	1.38	[76]

Table 5.2.: %ARD values for the heterosegmental PC-SAFT predictions for the binary systems butane - butanol and butanol - undecane shown in figure 5.2. N_{data} indicates the number of data points.

Figure 5.1 shows the vapor pressure of three n-alcohols with differing number of C-atoms dependent on the temperature. The heterosegmental PC-SAFT predictions are plotted parallel to experimental data given in the literature. Experimental data indicates that an increase in chain length leads to a decrease in vapor pressure, and that the vapor pressure exhibits a logarithmic relationship with the temperature. These empirical observations are consistent with the predictions of the model. Moreover, the %ARD values given in table 5.1 show a good agreement between model results and experimental data. Minor disparities in the %ARD values compared to Haarmann's values [56] can be attributed to the use of different experimental data and temperature ranges. In this work, alcohols are modeled by applying a 2B association scheme (see Table 3.1). The PC-SAFT parameters for the alkyl residue and the ($-CH_2OH$) head domain are taken from [56].

To validate the implementation of the heterosegmental PC-SAFT approach for binary systems, the model results for butanol-butane and butanol-undecane mixtures are compared with experimental data as shown in figure 5.2. The results are given in the form of the pressure of the mixture as a function of the composition. The low %ARDs presented in table 5.2 indicate very good consistence between model results and experimental data for both systems. The model accurately predicts the vapor pressure of the mixture and the composition of the vapor phase.

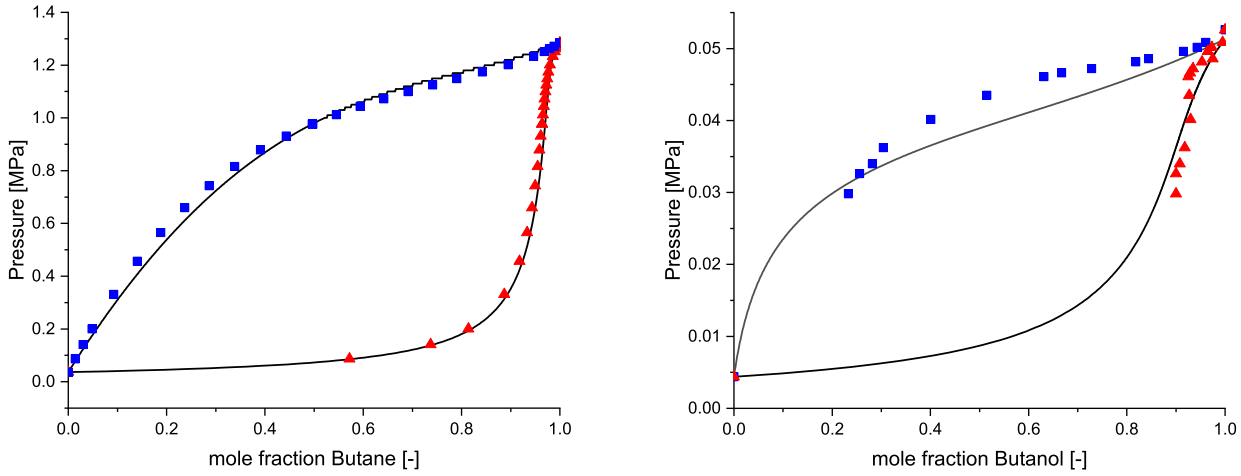

(a) Butane and Butanol at 364.5 K **(b)** Undecane and Butanol at 373.12 K

Figure 5.2.: Comparison of the heterosegmental PC-SAFT predictions for binary alkane-alcohol systems with experimental data (bubble point curve: blue squares; dew curve: red triangles)

5.2. Binary alkane - alcohol systems

As Haarmann et al. [56] already demonstrated that the heterosegmental PC-SAFT model is able to predict the thermodynamic behavior of alkane - alcohol systems, in the following, the model is applied to predict the pressure and mixture behavior of binary butane - alcohol systems and butanol - alkane systems. Phase diagrams provide valuable information for determining the appropriate operating conditions of technical processes and possible applications of the considered systems. In absorption processes for example, the solubility, as indicated by the maximum concentration achievable in a homogeneous solution, reflects the extent to which a substance in the gas phase can be effectively removed through absorption into the liquid phase [77].

Figure 5.3 shows the predicted pressure-composition phase diagrams for butane and three different alcohols at 350 K and at 400 K. The shape of the bubble point curve indicates positive deviation from Raoult's law for alcohols with a lower number of C-atoms (figure 5.3a and 5.3b), with the vapor pressure of the mixture being higher than expected for an ideal solution. This suggests that the intermolecular forces between butane and ethanol are weaker compared to the forces between butane - butane and ethanol - ethanol respectively. Consequently, the molecules of the components in the solution have a higher tendency to escape, resulting in each component having a partial vapor pressure greater than expected. For alcohols with higher number of C-atoms (figure 5.3e and 5.3f) this deviation becomes smaller and the behavior of the mixture approaches ideal

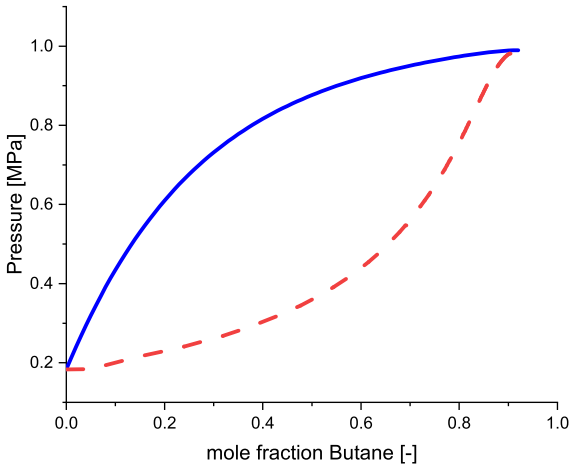

(a) Butane and Ethanol at 350 K

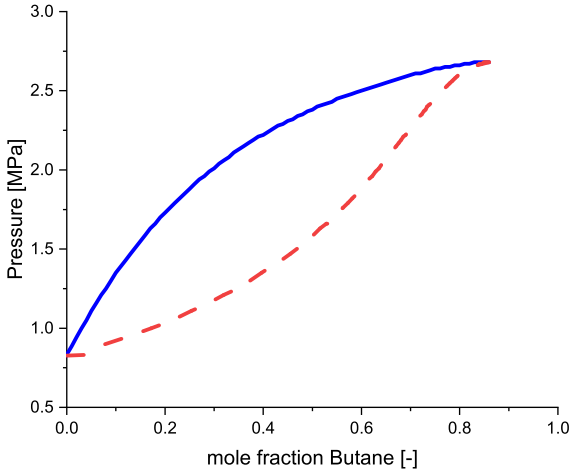

(b) Butane and Ethanol at 400 K

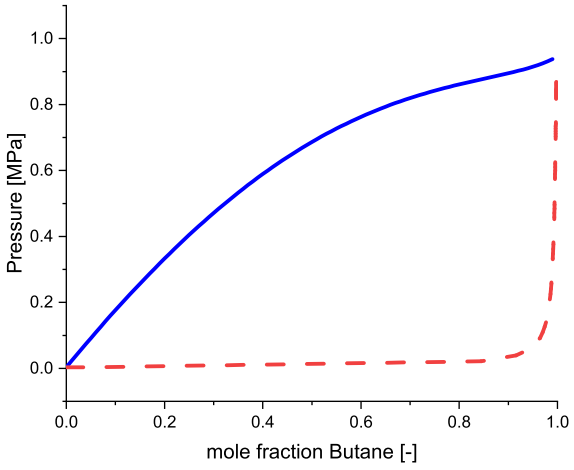

(c) Butane and Hexanol at 350 K

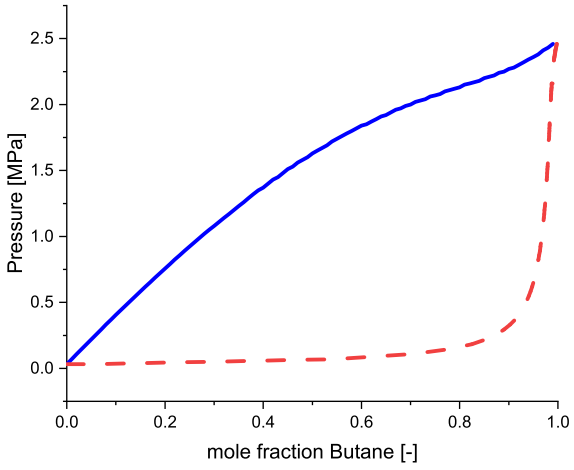

(d) Butane and Hexanol at 400 K

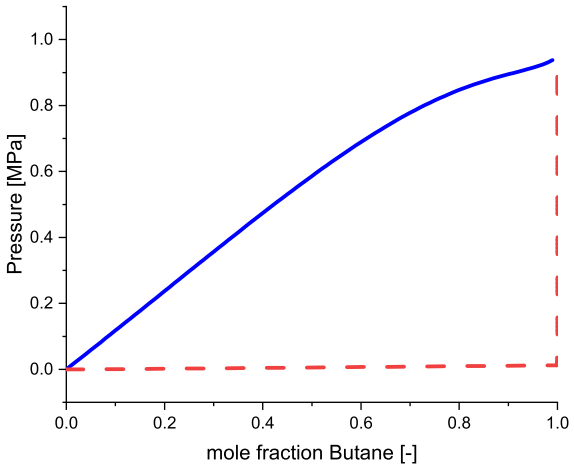

(e) Butane and Dodecanol at 350 K

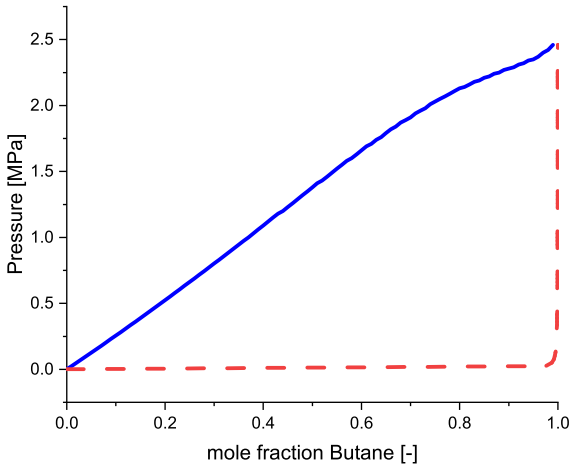

(f) Butane and Dodecanol at 400 K

Figure 5.3.: Heterosegmental PC-SAFT predictions for binary butane and alcohol systems at two different temperatures. (dew curve: red dashed line; bubble point curve: blue line)

behavior. As temperature increases, the miscibility gap or difference of liquid and vapor composition decreases in all systems, although this trend becomes less apparent with increasing number of C-atoms in the alcohol.
The almost vertical dew curve in butane - dodecanol systems (figure 5.3e and 5.3f), and the sudden transition from zero to approximately one, can be attributed to the significant difference in volatility between butane and dodecanol. At low pressures the two-phase region occupies a vast portion of the range, indicating immiscibility between the substances. The vapor phase consists mostly of the more volatile component butane. This is consistent with experimental data in a similar temperature range (e.g. [78]), indicating the predictive power of the heterosegmental PC-SAFT model for the miscibility of higher chain systems. Figure 5.4 illustrates the phase diagrams of butanol and three different alkanes at 350 K and 400 K, representing the pressure-composition relationship. The x-axis represents the mole fraction of the more volatile component, which is the alkane for the butane - butanol and hexane - butanol systems, while for dodecane - butanol mixtures, dodecane is the component with the lower boiling point, thus the mole fraction of butanol is plotted on the x-axis.
All three systems show positive deviations from Raoult's law. In the butanol - dodecane systems (figure 5.4 and figure 5.4f) this deviation is more pronounced at lower butanol-concentrations, the shape of the bubble point curve approximates ideal behavior at butanol-concentrations close to one.
As the temperature increases, the miscibility gap reduces in size for all three systems. The hexane - butanol system (5.4c and figure 5.4d) with an alkane containing an intermediate number of carbon atoms exhibits the smallest miscibility gap.

5.3. Binary alcohol - CO_2 systems

Figure 5.5 shows the model results of the heterosegmental PC-SAFT approach for three different CO_2 - alcohol systems at a lower and a higher temperature alongside the corresponding experimental data. In addition, the homosegmental PC-SAFT results for the CO_2 - ethanol system, obtained using binary interaction parameters listed by [4], are also presented. The comparison indicates that the model results are in good agreement with the experimental data at lower pressures, but show significant overprediction of pressure closer to the critical point. The extent of overprediction diminishes for all systems at higher temperatures. It is important to note that model results based on equations of states often exhibit significant deviations when approaching the critical point. This can be attributed to the sharp increase in density fluctuations near the critical point [79].
The %ARD values for the investigated systems are given in table 5.3. The $\%ARD_{\Delta y}$ of

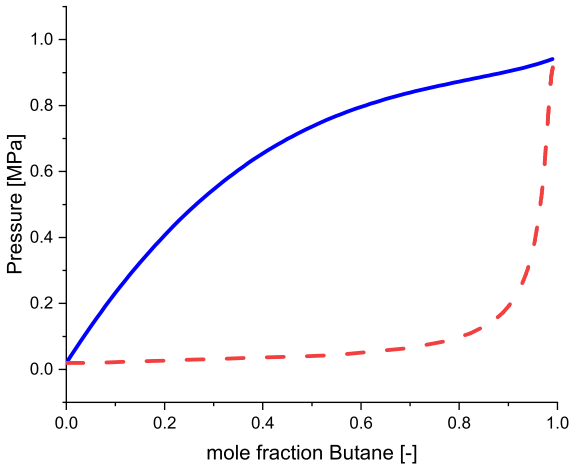

(a) Butane and Butanol at 350 K

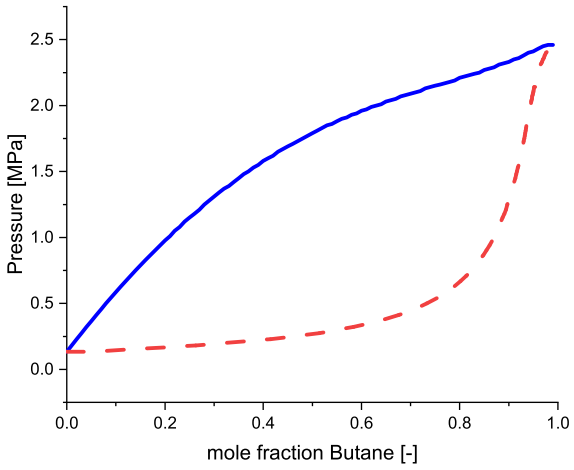

(b) Butane and Butanol at 400 K

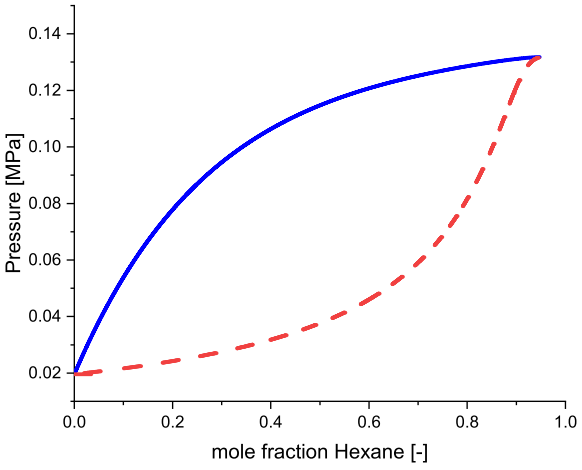

(c) Hexane and Butanol at 350 K

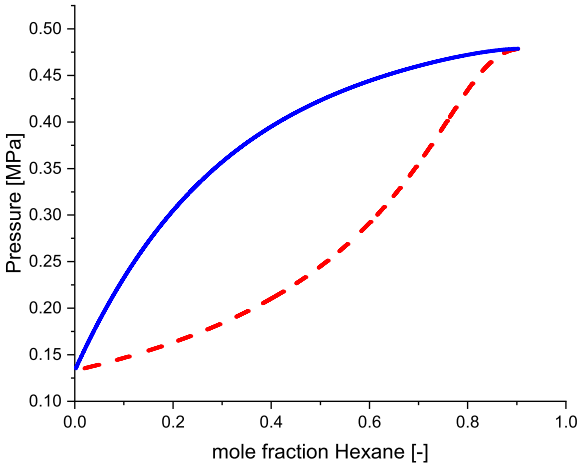

(d) Hexane and Butanol at 400 K

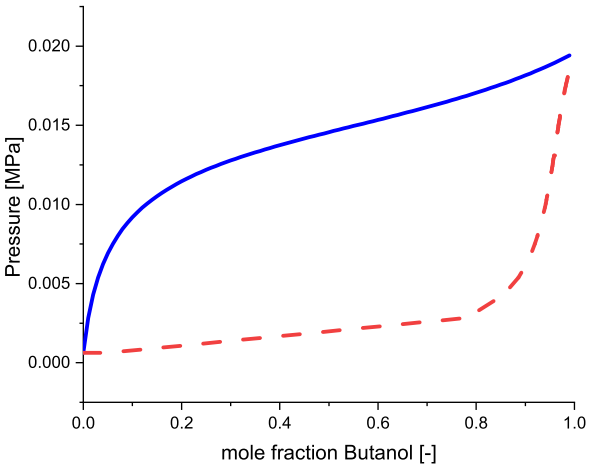

(e) Butanol and Dodecane at 350 K

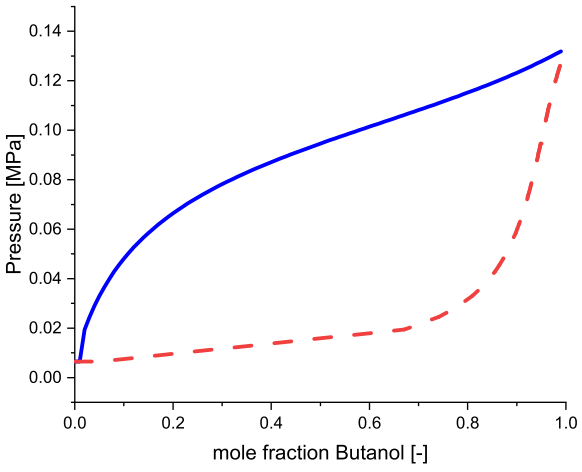

(f) Butanol and Dodecane at 400 K

Figure 5.4.: Heterosegmental PC-SAFT predictions for binary butanol and alkane systems at two different temperatures. (dew curve: red dashed line; bubble point curve: blue line)

CO_2 - hexanol systems are notably larger compared to the other systems, however this can be attributed to differences in the distribution of experimental data. In particular, the experimental data for CO_2 - hexanol systems comprise a larger number of data points close to the critical point than the other systems, leading to a more pronounced deviation of modeled results and experimental data. The same argument holds true for the higher $\%ARD_{\Delta y}$ of the CO_2 - dodecanol system at T = 392.2 K.
The experimental data indicates that the miscibility gap of CO_2 - ethanol systems decreases with increasing temperature, while this behavior is not observed for CO_2 - hexanol and CO_2 - dodecanol systems. Since the binary interaction parameter was fitted based on the CO_2 - octanol system, the model is not able to replicate this deviating behavior of the CO_2 - ethanol systems.
The comparison between the heterosegmental and homosegmental approaches for CO_2 - ethanol systems shows that the heterosegmental approach provides an improved fit to the experimental data in comparison to the homosegmental approach. Nevertheless, for the lower temperature (T = 353.15 K), the homosegmental approach appears to provide a better fit in the region closer to the critical point. However it is crucial to acknowledge that discrepancies between the models also stem from variations in the methodology employed to fit the binary parameters. Ramirez et al. [4] optimized the binary interaction parameters for the entire pressure range using vapor-liquid equilibrium data for alcohol - CO_2 systems from methanol to n-nonanol. In the present work the poor predictive ability of the PC-SAFT model at higher pressures was anticipated and only data points below 40% of the maximum experimental pressure were considered in the fitting process (cf. chapter 4.4.). Because of the distinct fitting methodologies, it is anticipated that the homosegmental approach utilizing the binary parameters provided in [4] would exhibit slightly better results in the critical region. On the other hand, the heterosegmental approach with binary parameters fitted as in this study is expected to exhibit better conformity with the experimental data at lower pressures.
The remarkable advantage of the heterosegmental approach however is its predictive capability. A single temperature-dependent binary parameter was fitted for the CO_2 - octanol system and then utilized for all the CO_2 - alcohol systems shown in figure 5.5. In contrast, for the homosegmental approach a temperature-dependent binary parameter has to be fitted for each individual CO_2 - alcohol system [4].

In this thesis, it was demonstrated that while neither the heterosegmental nor the homosegmental PC-SAFT model can accurately model the vapor-liquid equilibria of CO_2 - alcohol systems over the entire temperature and pressure range considered, fitting a single binary parameter for all systems using the heterosegmental approach resulted in comparable or even better results than the homosegmental approach, which requires fitting of multiple parameters. A possibility to improve the accuracy of the prediction

	System	T	N_{data}	$\%ARD_{\Delta p}$	$\%ARD_{\Delta y}$	$\%ARD_{\Delta p}$	$\%ARD_{\Delta y}$	ref
	CO_2 +	[K]	-	hetero	hetero	homo	homo	
(a)	Ethanol	353.15	12	2.98	5.36	4.14	15.01	[82]
(b)	Ethanol	391.96	9	8.85	5.91	6.46	30.27	[83]
(c)	Hexanol	353.15	13	0.39	50.67	-	-	[84]
(d)	Hexanol	397.78	11	1.13	54.54	-	-	[84]
(e)	Dodecanol	353.15	9	0.18	2.65	-	-	[85]
(f)	Dodecanol	393.2	6	0.85	10.63	-	-	[86]

Table 5.3.: %ARD values for the heterosegmental PC-SAFT predictions for the binary systems CO_2 and alcohols shown in figure 5.5. N_{data} indicates the number of data points.

would be to explore concentration-correlations of the binary interaction parameters. This was investigated by Villablanca-Ahues et al. [80] for n-Butanol - CO_2 systems for the homosegmental PC-SAFT, following the approach of Niño-Amézquita and Enders [81], who introduced a concentration-dependent binary parameter for methane - water systems. In this thesis, the incorporation of a second binary interaction parameter, as suggested by Ramirez et al. [4], did not yield satisfactory results in terms of reproducing the thermodynamic behavior of CO_2 - alcohol systems, opposed to the homosegmental approach.

5.4. Deviation in critical region in alkane - butanol systems

In their study, Haarmann et al. [56] showed that the PC-SAFT model accurately predicts the behavior of mixtures containing n-butanol and alkanes ranging from four to sixteen carbon atoms, as well as n-decanol with alkanes ranging from four to ten carbon atoms, with good agreement to experimental data. However, during the course of this thesis, it was observed that the ethane - butanol systems exhibit a similar pattern of deviation from experimental data as the CO_2 - alcohol systems discussed in Chapter 5.3. In figure 5.6a the comparison between the model results and experimental data for the ethane - butanol system is presented. Exactly like observed in the CO_2 - alcohol systems, the results show good agreement at lower pressure and butanol-concentrations, and overpredict the pressure close to the critical point of the mixture significantly. Similar trends can be observed in propane - butanol systems (figure 5.6b), although to a lesser extent. This deviation pattern is not present in butane - butanol systems, as shown in figure 5.2a.

For both the ethane - butanol and the propane - butanol systems, the binary parameters have been set to zero, following the approach adopted by Haarmann et al. [56] for alkane - alcohol systems.

These findings suggest that the observed deviation at higher pressures is not specific to systems with quadrupolar interactions. As discussed in chapter 5.3, the predictive capabilities of models generally decrease in the critical region of fluids due to their complex behavior [79]. This deviation is not observed in mixtures of butanol with alkanes containing higher numbers of carbon atoms, (see figure 5.4), although it is noteworthy, that butane, hexane and dodecane are below their respective critical points at the temperature investigated in this thesis, whereas ethane, propane, and CO_2 are above their critical points. However, this difference alone cannot explain the magnitude of deviations in the critical region, as the deviation is much greater in the ethane - butanol system compared to the propane - butanol system. Further investigations will be necessary to uncover the underlying reasons for this behavior.

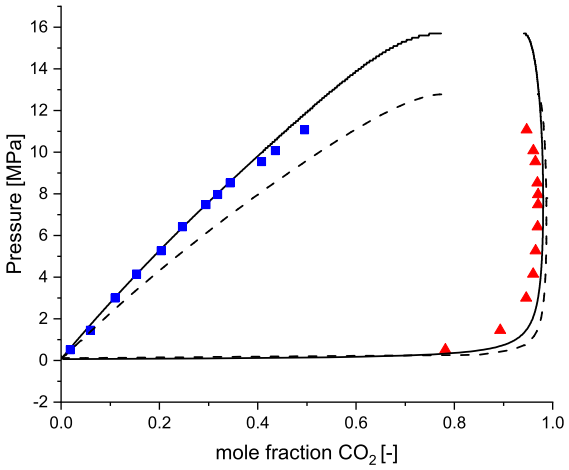

(a) CO_2 and Ethanol at 353.15 K

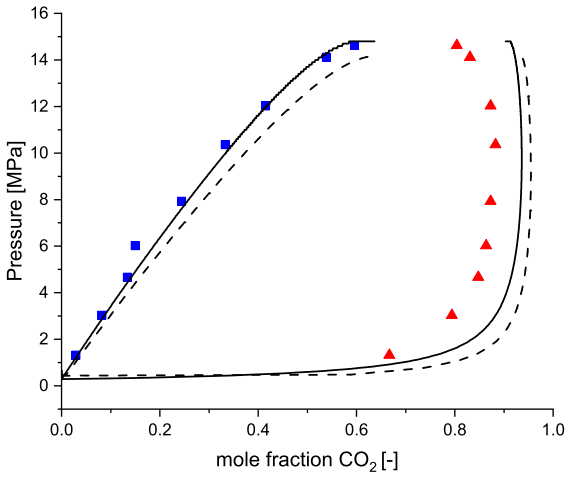

(b) CO_2 and Ethanol at 391.96 K

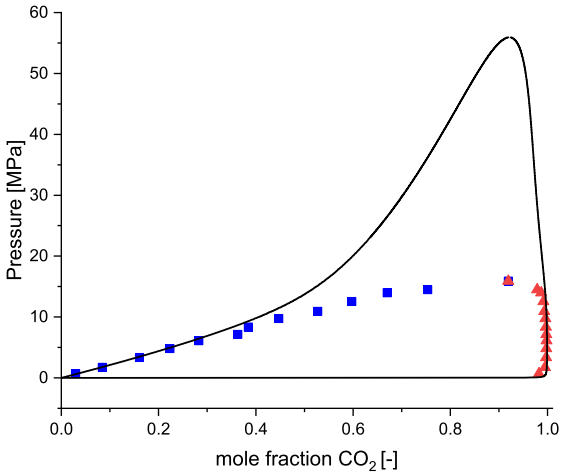

(c) CO_2 and Hexanol at 353.15 K

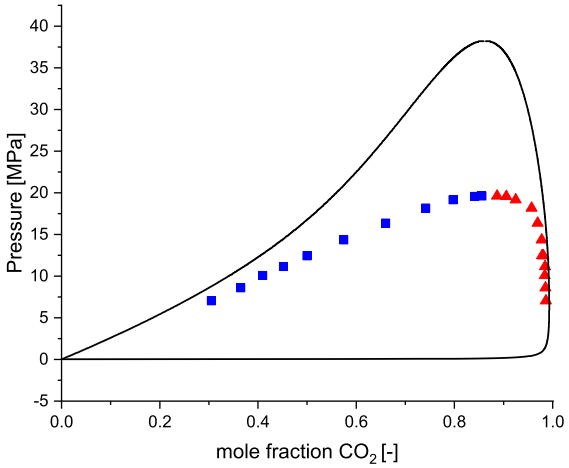

(d) CO_2 and Hexanol at 397.78 K

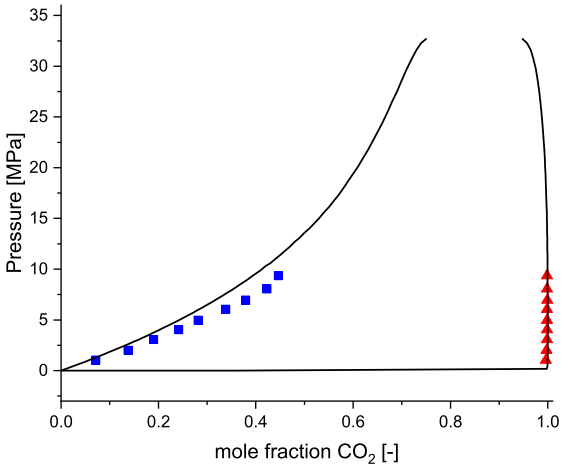

(e) CO_2 and Dodecanol at 353.15 K

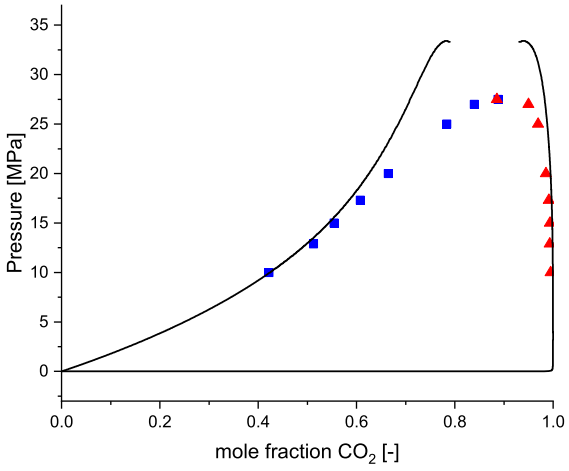

(f) CO_2 and Dodecanol at 393.2 K

Figure 5.5.: Comparison of the heterosegmental PC-SAFT predictions (solid line) for binary CO_2 - alcohol systems with experimental data (bubble point curve: blue squares; dew curve: red triangles. ref: see table 5.3) and the homosegmental PC-SAFT predictions (dashed line)

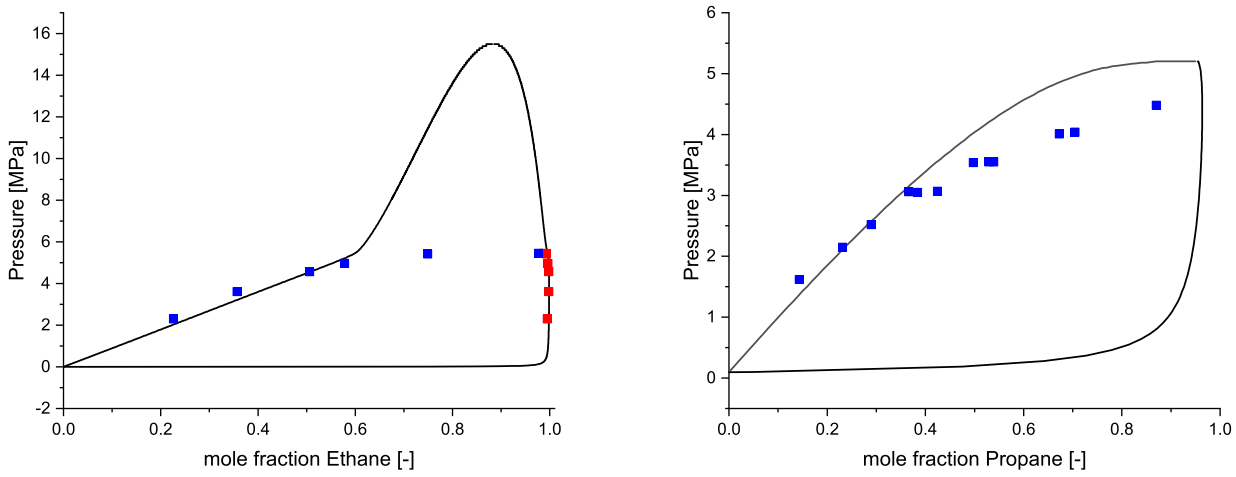

(a) Ethane and Butanol at 313.15 K

(b) Propane and Butanol at 390.8 K

Figure 5.6.: Comparison of the heterosegmental PC-SAFT predictions for (a) ethane - butanol [87] and (b) propane - butanol [88] systems with experimental data (bubble point curve: blue squares; dew curve: red triangles). There is no experimental data available for the dew curve of the propane-butanol system.

6. Conclusion

The objective of this thesis was to implement the heterosegmental Perturbed Chain Statistical Associating Fluid Theory (PC-SAFT) equation of state. The implementation was validated by modeling the same systems modeled by Haarmann et al. [56] utilizing the heterosegmental approach. The comparison of the modeling results with experimental phase equilibria data available in the literature showed good agreement for pure n-alcohol systems as well as binary alcohol - alkane mixtures.

Subsequently, the model was applied to predict the behavior of butane - ethanol, butane - hexanol and butane - dodecanol systems at two different temperatures. The results indicated that the miscibility gap expands with an increase in the number of carbon atoms in the alcohol and diminishes with rising temperature. Moreover, as the number of C-atoms increases, the mixture approaches the characteristics of an ideal solution. Moreover, the model was employed to simulate the binary systems of butane - butanol, hexane - butanol, and butanol - dodecane. The findings indicate that the miscibility gap decreases from butane to hexane, but expands again in the butanol - dodecane mixture. The size of the gap diminishes with increasing temperature for all systems.

For the purpose of modeling the thermodynamic behavior of n-alcohol - CO_2 systems, first the binary interaction parameters were obtained. The parameter correcting the alkyl residue - CO_2 interaction was assumed to be a constant independent of temperature and the number of C-atoms, consistent with previous research [58]. The binary parameter for the ($-CH_2OH$) - CO_2 interaction was adjusted to fit the vapor-pressure of CO_2 - octanol across a broad temperature range. A linear correlation with temperature was established for the parameter, which was assumed to be independent of the number of C-atoms of the alkyl residue of the alcohol molecule.

The evaluation of the results for CO_2 - alcohol systems obtained with the heterosegmental PC-SAFT model revealed its limited accuracy in modeling the complete pressure range of the studied systems. At lower pressure, the modeling results showed good agreement between calculation and experiment, while at higher pressures close to the critical region of the mixture, significant deviations were observed. These findings coincide with the results of the homosegmental approach as demonstrated by Ramirez et al. [4]. Although neither approach can precisely predict the vapor-liquid equilibria of CO_2 - alcohol systems across the entire temperature and pressure range investigated, fitting a single binary parameter for all systems using the heterosegmental approach resulted in comparable or superior outcomes relative to the homosegmental approach, which requires the fitting of multiple parameters.

To enable a quantitative comparison of the results obtained from both the homosegmental

and heterosegmental approaches, a consistent approach to fitting the binary interaction parameters should be implemented. Moreover, it is necessary to investigate a range of systems encompassing alcohols with various chain lengths across a wide temperature range.

While Haarmann et al. [56] reported good agreement between the heterosegmental PC-SAFT model results and experimental data for various n-alcohol - alkane systems, this thesis observed similar behavior to the CO_2 - alcohol systems in the modeling results of ethane - butanol and propane - butanol systems. These systems also exhibit an overprediction of pressure near the critical region, although the effect is more pronounced in the ethane - butanol systems. These findings suggest that this type of deviation is not solely attributed to the presence of quadrupolar interactions in the mixtures. Further research is needed to investigate the underlying reasons for these deviations.

Bibliography

[1] Joachim Gross and Gabriele Sadowski. “Perturbed-Chain SAFT: An Equation of State Based on a Perturbation Theory for Chain Molecules”. In: *Ind. Eng. Chem. Res.* 40 (2001), pp. 1244–1260.

[2] Walter Chapman, George Jackson, and Keith E. Gubbins. “Phase equilibria of associating fluids”. In: *Molecular Physics* 65:5 (1988), pp. 1057–1079.

[3] Joachim Gross et al. “Modeling Copolymer Systems Using the Perturbed-Chain SAFT Equation of State”. In: *Ind. Eng. Chem. Res.* 42 (2003), pp. 1266–1274.

[4] Luis A. Román-Ramírez et al. “Modeling of VaporLiquid Equilibria for CO2 + 1-Alkanol Binary Systems with the PC-SAFT Equation of State Using Polar Contributions”. In: *Ind. Eng. Chem. Res.* 49 (23 2010), pp. 12276–12283.

[5] Yunus Cengel, Michael Boles, and Mehmet Kanoglu. *Thermodynamics: An Engineering Approach*. McGraw-Hill Education, 2018.

[6] Christa Lüdecke and Dorothea Lüdecke. *Thermodynamik: Physikalisch-chemische Grundlagen der thermischen Verfahrenstechnik*. Springer Berlin Heidelberg, 2012.

[7] L. Chen. “Chemical potential and Gibbs free energy”. In: *MRS Bulletin* 44.7 (2019), pp. 520–523.

[8] Peter Atkins and Julio de Paula. *Physical Chemistry*. Oxford University Press, 2014.

[9] Ashok K. Singh. *Engineered Nanoparticles*. Academic Press, 2016.

[10] Erich A. Müller and Keith E. Gubbins. “Molecular-Based Equations of State for Associating Fluids: A Review of SAFT and Related Approaches”. In: *Ind. Eng. Chem. Res.* 40 (2001), pp. 2193–2211.

[11] Bennett D. Marshall. “Thermodynamic Perturbation Theory for Associating Fluids: Beyond First Order”. PhD thesis. Rice University, 2014.

[12] Phil Attard. *Chapter 7 - Interacting Particles, Thermodynamics and Statistical Mechanics*. Academic Press, 2002, pp. 153–179.

[13] B. J. Berne and P. Pechukas. “Gaussian model potentials for molecular interactions”. In: *The Journal of Chemical Physics* 56.7 (1972), pp. 3283–3296.

[14] Jacob N. Israelachvili. *Intermolecular and Surface Forces*. Academic Press, 2011.

[15] Francesco Sciortino. “Disorderd materials: One liquid, two glasses”. In: *Nature materials* 1 (2002), pp. 145–6.

[16] Walter W. Focke et al. “Revisiting the Classic Activity Coefficient Models”. In: *Industrial & Engineering Chemistry Research* 60.15 (2021), pp. 5639–5650.

[17] E. L. Cheluget, G. Wilczek-Vera, and J. H. Vera. “On the Relation Between Activity Coefficients and Excess Gibbs Energy Functions”. In: *The Canadian Journal of Engineering* 70 (1992), pp. 313–319.

[18] Øivind Wilhelmsen et al. “Thermodynamic Modeling with Equations of State: Present Challenges with Established Methods”. In: *Ind. Eng. Chem. Res.* 56 (2017), pp. 3503–3515.

[19] K.A. Masavetas. “The mere concept of an ideal gas”. In: *Mathematical and Computer Modelling* 12 (1989), pp. 651–657.

[20] Bruce E. Poling, John M. Prausnitz, and John P. O’Connell. *The Properties of Gases and Liquids*. 5th. McGraw-Hill, 2000.

[21] G. M. Kontogeorgis and G.K. Folas. *Thermodynamic Models for Industrial Applications - From Classical and Advanced Mixing Rules to Association Theories*. John Wiley & Sons., 2010.

[22] J. M. Prausnitz, R. N. Lichtenthaler, and E. G. Azevedo. *Molecular Thermodynamics of Fluid-Phase Equilibria*. 3rd. Prentice Hall, 1999.

[23] Michaela Heier et al. “Equation of state for the Lennard-Jones truncated and shifted fluid with a cut-off radius of 2.5 σ based on perturbation theory and its applications to interfacial thermodynamics”. In: *Molecular Physics* 116.15-16 (2018), pp. 2083–2094.

[24] Kai Langenbach. “Co-Oriented Fluid Functional Equation for Electrostatic interactions (COFFEE)”. In: *Chemical Engineering Science* 174 (2017).

[25] J. A. Barker and D. Henderson. “Perturbation Theory and Equation of State for Fluids: The Square-Well Potential”. In: *The Journal of Chemical Physics* 47.8 (1967), pp. 2856–2861.

[26] Mark Tuckerman. *Statistical Mechanics: Theory And Molecular Simulation*. Oxford University Press, 2001.

[27] W. Zmpitas and J. Gross. “Detailed pedagogical review and analysis of Wertheim’s thermodynamic perturbation theory”. In: *Fluid Phase Equilibria* 428 (2016), pp. 121–152.

[28] Michael S. Wertheim. “M.S. Fluids with highly directional attractive forces. I. Statistical thermodynamics”. In: *Journal of Statistical Physics* 35 (1984), pp. 19–34.

[29] Michael S. Wertheim. “Fluids with highly directional attractive forces. II. Thermodynamic perturbation theory and integral equations”. In: *Journal of Statistical Physics* 35 (1984), pp. 35–47.

[30] Michael S. Wertheim. “Fluids with highly directional attractive forces. III. Multiple attraction sites”. In: *Journal of Statistical Physics* 42 (1986), pp. 459–476.

[31] Michael S. Wertheim. “Fluids with highly directional attractive forces. IV. Equilibrium polymerization”. In: *Journal of Statistical Physics* 42 (1986), pp. 477–492.

[32] Walter G. Chapman et al. “New Reference Equation of State for Associating Liquids”. In: *Ind. Eng. Chem. Res.* 29 (1990), pp. 1709–1721.

[33] Stanley H. Huang and Maciej Radosz. “Equation of State for Small, Large, Polydisperse, and Associating Molecules”. In: *Ind. Eng. Chem. Res.* 29 (1990), pp. 2284–2294.

[34] Stanley H. Huang and Maciej Radosz. “Equation of State for Small, Large, Polydisperse, and Associating Molecules: Extension to Fluid Mixtures”. In: *Ind. Eng. Chem. Res.* 30 (1991), pp. 1994–2005.

[35] Ilke Senol. “Perturbed-Chain Statistical Association Fluid Theory (PC-SAFT) Parameters for Propane, Ethylene, and Hydrogen under Supercritical Conditions”. In: *World Academy of Science, Engineering and Technology* 59 (2011), pp. 1395–1403.

[36] Yuan-Hao Fu and Stanley I. Sandler. “A Simplified SAFT Equation of State for Associating Compounds and Mixtures”. In: *Ind. Eng. Chem. Res.* 34.5 (1995), pp. 1897–1909.

[37] Thomas Kraska and Keith E. Gubbins. “Phase Equilibria Calculations with a Modified SAFT Equation of State. 1. Pure Alkanes, Alkanols, and Water”. In: *Ind. Eng. Chem. Res.* 35.12 (1996), pp. 4727–4737.

[38] Thomas Kraska and Keith E. Gubbins. “Phase Equilibria Calculations with a Modified SAFT Equation of State. 2. Binary Mixtures of n-Alkanes, 1-Alkanols, and Water”. In: *Ind. Eng. Chem. Res.* 35.12 (1996), pp. 4738–4746.

[39] F. J. Blas and L. F. Vega. “Thermodynamic behaviour of homonuclear and heteronuclear Lennard-Jones chains with association sites from simulation and theory”. In: *Molecular Physics* 92.1 (1997), pp. 135–150.

[40] F. J. Blas and L. F. Vega. “Critical behavior and partial miscibility phenomena in binary mixtures of hydrocarbons by the statistical associating fluid theory”. In: *The Journal of Chemical Physics* 109.17 (1998), pp. 7405–7413.

[41] Alejandro Gil-Villegas et al. “Statistical associating fluid theory for chain molecules with attractive potentials of variable range”. In: *The Journal of Chemical Physics* 106.10 (1998), p. 4168.

[42] Joachim Gross and Gabriele Sadowski. “Modeling Polymer Systems Using the Perturbed-Chain Statistical Associating Fluid Theory Equation of State”. In: *Ind. Eng. Chem. Res.* 41 (2002), pp. 1084–1093.

[43] Joachim Gross and Gabriele Sadowski. “Application of the Perturbed-Chain SAFT Equation of State to Associating Systems”. In: *Ind. Eng. Chem. Res.* 41 (2002), pp. 5510–5515.

[44] Norman F. Carnahan and Kenneth E. Starling. “Equation of State for Nonattracting Rigid Spheres”. In: *The Journal of Chemical Physics* 51.2 (1969), p. 635.

[45] Thomas C Hales. “A proof of the Kepler conjecture”. In: *Annals of Mathematics* 162.3 (2005), pp. 1065–1185.

[46] Richard L Cotterman, Benjamin J Schwartz, and John M Prausnitz. “Molecular Thermodynamics for Fluids at Low and High Densities”. In: *AIChE Journal* 32.11 (1986), pp. 1787–1798.

[47] Andrés Santos, Santos B. Yuste, and Mariano López de Haro. “Structural and thermodynamic properties of hard-sphere fluids”. In: *J. Chem. Phys.* 153 (2020), p. 120901.

[48] Thomas M. Reed and Keith E. Gubbins. *Applied Statistical Mechanics*. McGraw-Hill, 1973.

[49] Joachim Gross. “An equation-of-state contribution for polar components: Quadrupolar molecules”. In: *AIChE Journal* 51.9 (2005), pp. 2556–2568.

[50] Stephen S. Chen and Aleksander Kreglewski. “Applications of the Augmented van der Waals Theory of Fluids”. In: *Berichte der Bunsengesellschaft für physikalische Chemie* 81.10 (1977), p. 1048.

[51] J. A. Barker and D. Henderson. “Perturbation Theory and Equation of State for Fluids. II. A Successful Theory of Liquids”. In: *J. Chem. Phys.* 47.11 (1967), p. 4714.

[52] Hu Y. Liu H. “Molecular thermodynamic theory for polymer systems II. Equation of state for chain fluids”. In: *Fluid Phase Equilib.* 122 (), pp. 75–97.

[53] Gray CG. Twu CH Gubbins KE. “Thermodynamics of mixtures of nonspherical molecules. III. Fluid phase equilibria and critical loci”. In: *J Chem Phys.* 64 (1976), pp. 5186–5197.

[54] D. Berthelot. “Sur les coefficients de dilatation des liquides homogènes”. In: *Annales de Chimie et de Physique* 13.6 (1898), pp. 385–404.

[55] Frank Bovey and Peter Mirau. *NMR of Polymers*. Academic Press, 1996.

[56] Niklas Haarmann, Sabine Enders, and Gabriele Sadowski. “Heterosegmental Modeling of Long-Chain Molecules and Related Mixtures using PC-SAFT: 2. Associating Compounds”. In: *Ind. Eng. Chem. Res.* 58 (2019), pp. 4625–4643.

[57] Niklas Haarmann, Sabine Enders, and Gabriele Sadowski. “Heterosegmental Modeling of Long-Chain Molecules and Related Mixtures using PC-SAFT: 1. Polar Compounds”. In: *Ind. Eng. Chem. Res.* 58 (2019), pp. 2551–2574.

[58] Alfonso Gonzalez Perez et al. “Comparative study of vapour-liquid equilibrium and density modelling of mixtures related to carbon capture and storage with the SRK, PR, PC- SAFT and SAFT-VR Mie equations of state for industrial uses”. In: *Fluid Phase Equilibria* 440 (2017), pp. 19–35.

[59] J. T. Chen W. L. Weng and M. J. Lee. “High-Pressure Vapor-Liquid Equilibria for Mixtures Containing a Supercritical Fluid”. In: *Ind. Eng. Chem. Res.* 33 (1994).

[60] S. Ahmad, R. Giesen, and K. Lucas. “Vapor-Liquid Equilibrium Studies for Systems Containing n-Butylisocyanate at Temperatures between 323.15 K and 371.15 K”. In: *J. Chem. Eng. Data* 49 (3 2004), pp. 826–831.

[61] J. Linek. “Isothermal and Isobric Vapor-Liquid Equilibrium Data in the Tetrachloromethane-n-Butyl Alcohol System”. In: *Collect. Czech. Chem. Commun.* 48 (11 1983), pp. 2879–2887.

[62] J. Ortega et al. “Thermodynamic Study on Binary Mixtures of Propyl Ehtanoate and an Alkan-1-ol (C2-C4): Isobaric Vapor-Liquid Equilibria and Excess”. In: *Fluid Phase Equilib.* 170 (1-2 2000), pp. 87–111.

[63] P. Susial et al. “Isobaric (Vapor+Liquid) Equilibrium for n-Propyl Acetate with 1-Butanol or 2-Butanol”. In: *Fluid Phase Equilib.* 385 (2015), pp. 196–204.

[64] W. B. Kay and W. E. Donham. “Liquid-Vapor Equilibrium in the Isobutyl Alcohol-Butanol, Methanol-Butanol, and Diethyl Ether-Butanol Systems”. In: *Chem. Eng. Sci.* 4 (1 1955), pp. 1–16.

[65] K. Nasirzadeh, R. Neueder, and W. Kunz. “Vapor Pressure Determination of the Aliphatic C5 to C8 1-Alcohols”. In: *Journal of Chemical & Engineering Data* 51.1 (2006), pp. 7–10.

[66] Alexandra Brozena. “Vapor pressure of 1-octanol below 5 kPa using DSC”. In: *Thermochimica Acta* 561 (2013), pp. 72–76.

[67] Yan Wang et al. “Measurement and correlation of the vapor pressure of a series of α-pinene derivatives”. In: *Journal of Chemical & Engineering Data* 59.2 (2014), pp. 494–498.

[68] D. Ambrose and CHS Sprake. “Thermodynamic properties of organic oxygen compounds XXV. Vapor pressures and normal boiling temperatures of aliphatic alcohols”. In: *The Journal of Chemical Thermodynamics* 2.6 (1970), pp. 631–645.

[69] D. Ambrose and CHS Sprake. “Thermodynamic properties of organic oxygen compounds XXV. Vapor pressures and normal boiling temperatures of aliphatic alcohols”. In: *The Journal of Chemical Thermodynamics* 2.6 (1970), pp. 631–645.

[70] G. Geiseler et al. “Physical properties of position isomer n-dodecanols”. In: *Zeitschrift für Physikalische Chemie* 220 (1962), p. 79.

[71] D. Ambrose, JH Ellender, and CHS Sprake. “Thermodynamic properties of organic oxygen compounds. XXXV. Vapor pressures of aliphatic alcohols”. In: *The Journal of Chemical Thermodynamics* 6.10 (1974), pp. 909–914.

[72] George S Parks and Richard D Rowe. “The heats of solution of hexamethylbenzene, cetyl alcohol, and dicetyl in related liquids; heats of fusion by an extrapolation process”. In: *The Journal of Chemical Physics* 14.8 (1946), pp. 507–510.

[73] J Schmelzer et al. “Vapour-liquid equilibria and heats of mixing in n-alkane-1-alcohol systems. III. Vapour-liquid equilibria in n-alkane-1-dodecanol systems”. In: *Fluid Phase Equilibria* 15 (1983), pp. 107–119.

[74] D Ambrose and CHS Sprake. “Thermodynamic properties of organic oxygen compounds XXV. Vapor pressures and normal boiling temperatures of aliphatic alcohols”. In: *The Journal of Chemical Thermodynamics* 2.5 (1970), pp. 631–645.

[75] C. Dell’Era et al. “High-pressure phase equilibria of butanol isomers with n-alkanes: Experimental data and modelling”. In: *Fluid Phase Equilibria* 254 (2007), pp. 49–59.

[76] J Schmelzer et al. “Vapor-liquid equlibria and heats of mixing in alkane + 1-alcohol systems: I. vapor-liquid equilibria in 1-alcohol + undecane systems”. In: *Fluid Phase Equilibria* 11 (1983), pp. 187–200.

[77] I Ubong, N Harry-Ngei, and PN Ede. “A Review of Solvent Selection Considerations in Absorption Systems”. In: *European Journal of Engineering and Technology Research* 4.11 (2019), pp. 5–10.

[78] A. Belabbaci et al. “Vapor-Liquid Equilibria of Binary Mixtures Containing 1-Butanol and Hydrocarbons at 313.15 K”. In: *Journal of Chemical Engineering Data* 57 (2012), pp. 114–119.

[79] Meijie Yang et al. “Crossover PC-SAFT equations of state based on White’s method for the thermodynamic properties of CO2, n-alkanes and n-alkanols”. In: *Fluid Phase Equilibria* 564 (2023), p. 113610.

[80] R. Villablanca-Ahues et al. “Interfacial tension and phase equilibria for binary systems containing (CH4-CO2)+(n-dodecane; n-butanol; water)”. In: *Fluid Phase Equilibria* 570 (2023).

[81] Oscar Gabriel Niño-Amézquita and Sabine Enders. “Phase equilibrium and interfacial properties of water+methane mixtures”. In: *Fluid Phase Equilibria* 407 (2016), pp. 143–151.

[82] C. Secuianu, V. Feroiu, and D. Geancentsa. “Phase behavior for carbon dioxide + ethanol system: Experimental measurements and modeling with a cubic equation of state”. In: *The Journal of Supercritical Fluids* 47.1 (2008), pp. 109–116.

[83] J. L. Mendoza de la Cruz and L. A. Galicia-Luna. “ELDATA: The International Electronic Journal of Physico-Chemical Data”. In: *ELDATA* 5 (1999), pp. 157–164.

[84] O. Elizalde-Solis et al. “Vapor-liquid equilibria and critical points of the CO2 + 1-hexanol and CO2 + 1-heptanol systems”. In: *Fluid Phase Equilib.* 210 (2003), pp. 215–227.

[85] A. Kordikowski and G. M. Schneider. “Fluid Phase Equilibria”. In: *Fluid Phase Equilib.* 90 (1993), pp. 149–162.

[86] M. Spee and G. M. Schneider. “Fluid Phase Equilibria”. In: *Fluid Phase Equilib.* 65 (1991), pp. 263–274.

[87] Daiki Kodama et al. “High pressure phase equilibrium properties for ethane + 1-butanol system at 313.15 K”. In: *Fluid Phase Equilibria* 201 (2002), pp. 401–407.

[88] C. Borch-Jensen, A. Staby, and J. Mollerup. “Mutual solubility of 1-butanol and carbon dioxide, ethene, ethane, or propane at a reduced supercritical solvent temperature of 1.03”. In: *J. Supercrit. Fluids* 7 (1994), pp. 231–244.

List of Symbols

ϵ	depth of pair potential, J
η	packing fraction, $\eta = \zeta_3$
γ	activity coefficient
λ	reduced well width of square-well potential
μ	chemical potential, $\mathrm{J\,mol^{-1}}$
Φ	pair potential, J
ρ	total number density of molecules, $\mathrm{Å^{-3}}$
σ	segment diameter, Å
a	Helmholtz free energy, J
a_i, b_i	universal model constants for PC-SAFT
d	temperature dependent segment diameter, Å
E	total energy, J
f	fugacity, Pa
G^E	excess Gibbs energy, J
g^{hs}	radial distribution function
k_B	Boltzmann's constant, $\mathrm{J\,K^{-1}}$
k_{ij}	binary parameter
m	number of segments
N_{Av}	Avogadro's constant, $\mathrm{mol^{-1}}$
p	pressure, Pa
Q	partition function
S	entropy, $\mathrm{J\,K^{-1}}$
T_R	reduced temperature
U	internal energy, J
v	molar volume, $\mathrm{m^3\,mol^{-1}}$
X	mole fraction not bonded at association site
x	mole fraction
Z	compressibility factor

List of Figures

List of Tables

A. Heterosegmental PC-SAFT equations

A.1. Chain contribution

$$\tilde{a}^{hs} = \frac{1}{\zeta_0}\left[\frac{3\zeta_1\zeta_2}{(1-\zeta_3)} + \frac{(\zeta_2)^3}{\zeta_3(1-\zeta_3)^2} + \left(\frac{(\zeta_2)^3}{(\zeta_3)^2} - \zeta_0\right)\ln(1-\zeta_3)\right] \tag{A.1}$$

$$\tilde{a}^{hc} = \bar{m}\tilde{a}^{hs} - \sum_i x_i(1-m_i)\sum_\alpha\sum_\beta B_{i\alpha i\beta}\ln\left[g_{i\alpha i\beta}(d_{i\alpha i\beta})\right] \tag{A.2}$$

It should be noted that the last summations of the equation as it is given here can only be applied in combination with the bonding fractions defined by Gross et al. (Table 3.4). In Haarmann's modification of the equation [57][56], mixed indices are considered only once.

A.2. Dispersion contribution

$$\begin{aligned}\tilde{a}^{disp} = &-2\pi\rho I_1(\bar{m},\eta)\sum_i\sum_j x_i x_j m_i m_j \sum_\alpha\sum_\beta z_{i\alpha}z_{j\beta}\left(\frac{\epsilon_{i\alpha j\beta}}{kT}\right)\sigma^3_{i\alpha j\beta} - \\ &\pi\rho\bar{m}\left(1 + Z^{hc} + \rho\frac{\partial Z^{hc}}{\partial\rho}\right)^{-1} I_2(\bar{m},\eta) \\ &\sum_i\sum_j x_i x_j m_i m_j \sum_\alpha\sum_\beta z_{i\alpha}z_{j\beta}\left(\frac{\epsilon_{i\alpha j\beta}}{kT}\right)^2\sigma^3_{i\alpha j\beta}\end{aligned} \tag{A.3}$$

A.3. Association contribution

$$g_{i\alpha j\beta}(d_{i\alpha j\beta}) = \frac{1}{1-\zeta_3} + \frac{3d_{i\alpha}d_{j\beta}}{d_{i\alpha}+d_{j\beta}}\frac{\zeta_2}{(1-\zeta_3)^2} + 2\left[\frac{d_{i\alpha}d_{j\beta}}{d_{i\alpha}+d_{j\beta}}\right]^2\frac{(\zeta_2)^2}{(1-\zeta_3)^3} \tag{A.4}$$

$$\Delta^{A_{i\alpha}B_{j\beta}} = (d_{i\alpha j\beta})^3 g_{i\alpha j\beta}(d_{i\alpha j\beta})\kappa^{A_{i\alpha}B_{j\beta}}\Delta^{A_{i\alpha}B_{j\beta}}\left[\exp\frac{\epsilon^{A_{i\alpha}B_{j\beta}}}{kT} - 1\right] \tag{A.5}$$

$$X^{A_{i\alpha}} = [1 + \rho\sum_j x_j\sum_\beta\sum_B X^{B_{j\beta}}\Delta^{A_{i\alpha}B_{j\beta)}}]^{-1} \tag{A.6}$$

$$\tilde{a}^{assoc} = \sum_i x_i\sum_\alpha\left[\sum_{A_{i\alpha}}\left(\ln X^{A_{i\alpha}} - \frac{X^{A_{i\alpha}}}{2}\right) + \frac{M_{i\alpha}}{2}\right] \tag{A.7}$$

A.4. Quadrupole contribution

$$\tilde{a}^{quad} = \frac{\tilde{a}_2}{1 - \tilde{a}_3/\tilde{a}_2} \tag{A.8}$$

$$\tilde{a}_2 = -\pi \left(\frac{3}{4}\right)^2 \rho \sum_i \sum_j x_i x_j \sum_\alpha \sum_\beta \frac{\epsilon_{i\alpha}}{k_B T} \frac{\epsilon_{j\beta}}{k_B T} \frac{\sigma_{i\alpha}^5 \sigma_{j\beta}^5}{\sigma_{i\alpha j\beta}^7} n_{Q,i\alpha} n_{Q,j\beta} Q^{*2}_{i\alpha} Q^{*2}_{j\beta} J_{2,i\alpha j\beta} \tag{A.9}$$

$$\begin{aligned}\tilde{a}_3 = \frac{\pi}{3} \left(\frac{3}{4}\right)^3 \rho \sum_i \sum_j x_i x_j \sum_\alpha \sum_\beta \left(\frac{\epsilon_{i\alpha}}{k_B T}\right)^{3/2} \left(\frac{\epsilon_{j\beta}}{k_B T}\right)^{3/2} \frac{\sigma_{i\alpha}^{15/2} \sigma_{j\beta}^{15/2}}{\sigma_{i\alpha j\beta}^{12}} \\ \times n_{Q,i\alpha} n_{Q,j\beta} Q^{*3}_{i\alpha} Q^{*3}_{j\beta} J_{3,i\alpha j\beta} + \frac{4\pi^2}{3} \left(\frac{3}{4}\right)^3 \rho^2 \sum_i \sum_j \sum_k x_i x_j x_k \end{aligned} \tag{A.10}$$

$$\times \sum_\alpha \sum_\beta \frac{\epsilon_{i\alpha}}{k_B T} \frac{\epsilon_{j\beta}}{k_B T} \frac{\epsilon_{k\gamma}}{k_B T} \frac{\sigma_{i\alpha}^5 \sigma_{j\beta}^5 \sigma_{k\gamma}^5}{\sigma_{i\alpha j\beta}^3 \sigma_{i\alpha k\gamma}^3 \sigma_{j\beta k\gamma}^3} n_{Q,i\alpha} n_{Q,j\beta} n_{Q,k\gamma} Q^{*2}_{i\alpha} Q^{*2}_{j\beta} Q^{*2}_{k\gamma} J_{3,i\alpha j\beta k\gamma}$$

$$Q^{*2}_{i\alpha} = \frac{Q_{i\alpha}^2}{m_{i\alpha} \epsilon_{i\alpha i\beta} \sigma_{i\alpha i\beta}^5} \tag{A.11}$$

$$J_{2,i\alpha j\beta} = \sum_{n=0}^{4} \left(a_{n,i\alpha j\beta} + b_{n,i\alpha j\beta} \frac{\epsilon_{i\alpha j\beta}}{k_B T}\right) \eta^n \tag{A.12}$$

$$J_{3,i\alpha j\beta k\gamma} = \sum_{n=0}^{4} c_{n,i\alpha j\beta k\gamma} \eta^n \tag{A.13}$$

$$J_{3,i\alpha j\beta} = 0 \tag{A.14}$$

$$a_{n,i\alpha j\beta} = a_{0n} + \frac{m_{i\alpha j\beta} - 1}{m_{i\alpha j\beta}} a_{1n} + \frac{m_{i\alpha j\beta} - 1}{m_{i\alpha j\beta}} \frac{m_{i\alpha j\beta} - 2}{m_{i\alpha j\beta}} a_{2n} \tag{A.15}$$

$$b_{n,i\alpha j\beta} = b_{0n} + \frac{m_{i\alpha j\beta} - 1}{m_{i\alpha j\beta}} b_{1n} + \frac{m_{i\alpha j\beta} - 1}{m_{i\alpha j\beta}} \frac{m_{i\alpha j\beta} - 2}{m_{i\alpha j\beta}} b_{2n} \tag{A.16}$$

$$c_{n,ijk} = c_{0n} + \frac{m_{i\alpha j\beta k\gamma} - 1}{m_{i\alpha j\beta k\gamma}} c_{1n} + \frac{m_{i\alpha j\beta k\gamma} - 1}{m_{i\alpha j\beta k\gamma}} \frac{m_{i\alpha j\beta k\gamma} - 2}{m_{i\alpha j\beta k\gamma}} c_{2n} \tag{A.17}$$

$$m_{i\alpha j\beta} = (m_{i\alpha} m_{j\beta})^{1/2} \tag{A.18}$$

$$m_{i\alpha j\beta k\gamma} = (m_{i\alpha} m_{j\beta} m_{k\gamma})^{1/3} \tag{A.19}$$